Effects of Climate Change on Runoff Dynamics in Alpine Catchments

Sarah Hanus

TU Delft

MSc Thesis Water Management

Effects of Climate Change on Runoff Dynamics in Alpine Catchments

by
Sarah Hanus

to obtain the degree of Master of Science
at the faculty of Civil Engineering and Geosciences at Delft University of Technology,
to be defended publicly on Tuesday October 27, 2020 at 9.00 AM.

Student number:	4796675	
Project Duration:	1.2.2020 - 27.10.2020	
Thesis committee:	Dr. Markus Hrachowitz	TU Delft (Chair)
	Dr. Gerrit Schoups	TU Delft
	Dr. Miren Vizcaino	TU Delft
	Dr. Harry Zekollari	TU Delft

An electronic version of this thesis is available at http://repository.tudelft.nl/.

Font page: Defreggental, Austria (Philipp Aigner, BOKU Wien)

TU Delft

Preface

For this thesis, I embarked on the journey of programming a hydrological model myself, determined to learn new skills and contribute to a better understanding of climate change impacts on hydrology. I have learned so much in these past eight months and I have discovered my joy for hydrological research.

This would not have been possible without the support of Markus. Thanks a lot for all your input, for always making time for Skype calls and for sharing your passion for hydrology, not only during the thesis, but especially during the courses of the Master programme. I also want to thank Gerrit, Harry and Miren for being part of my thesis committee, for taking time to read my thesis and adding value to it through critical input. Thanks as well to Roland for providing me with all necessary data and information concerning my study catchments and for your interest in this study.

My time in Delft would not have been as much fun and memorable without my friends. Thanks for spending the last two years with me, especially Fay, Vita, Sanne and Board 64 & 65 of the Dispuut Water & Environment.

A special thanks to Jan for his unconditional support throughout years, for giving me strength when I needed it most and for believing in me even when I don't myself. I am very grateful to have you in my life.

Lastly, I want to thank my parents for supporting me throughout my life.

Sarah Hanus
Delft, October 2020

Abstract

Hydrological regimes of alpine catchments are expected to be strongly influenced by climate change due to their dependence on snow dynamics. While seasonal changes have been studied extensively, studies on changes in the timing and magnitude of annual extremes remain rare. This study investigates the effects of climate change on runoff patterns in six alpine catchments in Austria by using a topography-driven semi-distributed hydrological model and 14 climate projections for both RCP 4.5 and RCP 8.5. The study catchments represent a range of alpine catchments, from pluvial-nival to nivo-glacial, as the study focuses on exploring the effects of climate change on catchments of different altitudes. Simulations of 1981-2010 were compared to projections of 2071-2100 and changes in timing and magnitude of annual maximum and minimum flows as well as monthly discharges and melt were examined. Our results indicate a substantial shift to earlier occurrences in annual maximum flows by 9 to 31 days and an extension of the potential flood season by 1 to 3 months for high elevation catchments. For lower elevation catchments, changes in timing of annual maximum flows are less pronounced. Magnitudes of annual maximum flows are likely to increase, with four catchments exhibiting larger increases under RCP 4.5 than RCP 8.5. The timing of minimum annual discharges shifts to earlier in the winter months for high elevation catchments, whereas for lower elevation catchments a shift from winter to autumn is observed. While all catchments show an increase in mean magnitude of minimum flows under RCP 4.5, this is only the case for four catchments under RCP 8.5. Our results suggest a relationship between the altitude of catchments and changes in timing of annual maximum and minimum flows and magnitude of low flows, whereas no relationship between altitude and magnitude of annual maximum flows could be distinguished. The degree of future change in timing and monthly discharges is larger under RCP 8.5, a change of up to twice as large in monthly discharges is found for RCP 8.5 compared to RCP 4.5.

1 Introduction

The hydrological cycle is impacted by climate change due to rising temperatures and changing precipitation patterns. Higher temperatures lead to rising potential evaporation and changes in snow dynamics which affect runoff processes. Changes in runoff patterns can be observed for the past, e.g. trends in timing and magnitude of floods (Blöschl et al., 2017, 2019) and subseasonal trends in runoff (Kormann et al., 2015). Special attention in regard to climate change should be given to high elevation areas because their hydrological regimes are strongly influenced by snow dynamics and changes in glaciated areas which makes them especially vulnerable to climate change (IPCC, 2019). The Alps have shown twice the average worldwide temperature increase in the last century (Brunetti et al., 2009). In alpine regions monthly runoff is characterised by a strong seasonality with maximum discharges in spring and summer and minimum discharges in winter. Also, annual extremes show a strong seasonality, with low flows in winter and maximum discharges mainly occurring during the snow melt season. Changes in seasonality of alpine hydrology has possible socio-economic as well as ecological implications, ranging from hydropower production (Schaefli et al., 2019), water availability (Barnett et al., 2005) to flooding and ecohydrology (Cauvy-Fraunié & Dangles, 2019). Hence, it is important to investigate in which direction and by which magnitude seasonal patterns in runoff are expected to change in future. Hydrological changes in the past indicate a positive trend in spring runoff and a negative trend in summer runoff in the Alpine region, with trend timing depending on the altitude of the catchments (Kormann et al., 2015). Hydrological low flows in high alpine catchments show a positive trend in the past (Laaha et al., 2016).

To investigate impacts of future climate change on hydrology, general circulation models (GCMs) with different emission scenario inputs are used as boundary conditions at a regional level for regional climate models (RCMs). The resulting temperature and precipitation data are utilized as inputs for hydrological models. Numerous studies were conducted using this methodology (e.g. Aich et al. (2014) for Africa, Marx et al. (2018) for Europe, Leng et al. (2015) for China), with several focusing on future changes in Alpine regions. Snow mass and snow cover duration are expected to reduce in the Alps in future (Bavay et al., 2013; Laghari et al., 2012; Marty et al., 2017). As a result, summer low flows are expected to decrease in catchments in Switzerland (Jenicek et al., 2018). However, in general hydrological low flows are predicted to increase in the Alps because winter low flows increase due to changes in snow dynamics related to increased temperatures (Laaha et al., 2016; Laurent et al., 2020; Marx et al., 2018; Parajka et al., 2016). Regarding annual floods, Köplin et al. (2014) predict an increased magnitude and a decreased seasonality for nival alpine catchments in Switzerland in the future.

In Austria, studies project an increase in winter flows and decrease in summer flows (Goler et al., 2016; Hanzer et al., 2018; Holzmann et al., 2010; Laghari et al., 2012; Tecklenburg et al., 2012) with the largest increases in winter flows found in high elevation areas (Stanzel & Nachtnebel, 2010). For the spring runoff

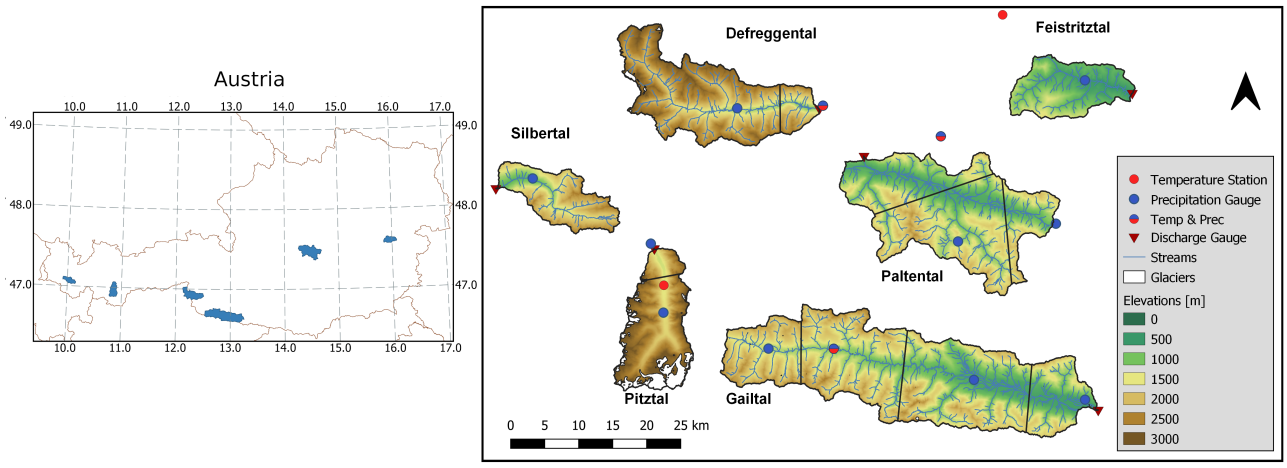

Figure 1: Outlines of catchments used in this study, showing elevations, the precipitation and temperature stations as well as the division into several precipitation zones illustrated by the black lines.

Table 1: Catchment characteristics. The discharge regimes are based on Mader et al. (1996).

	Silbertal	Pitztal	Defreggental	Gailtal	Paltental	Feistritztal
Area [km^2]	100	166	267	587	370	116
Elevation [m]	671-2764	1339-3763	1096-3485	596-2778	633-2447	449-1595
Mean Altitude[m]	1776	2558	2233	1476	1315	917
Discharge Regime	nival	nivo-glacial	nival	Autumn nival	Moderate nival	nivo-pluvial
Bare (Glacier) [%]	20 (0)	70 (18)	43 (1.5)	8 (0)	4 (0)	0 (0)
Grass [%]	46	23	32	33.5	32	25
Forest [%]	32	6	23	56.5	61	72
Riparian [%]	2	1	2	2	3	3
Nr Prec. Gauges	1	2	2	4	3	1

an inconsistent future trend over Austria is projected with increases in high alpine areas in western Austria (Stanzel & Nachtnebel, 2010; Tecklenburg et al., 2012) and decreases elsewhere (Laghari et al., 2012). Holzmann et al. (2010) assessed changes in high flows in future, showing a decrease in high flows in western Austria and an increase in eastern Austria. Goler et al. (2016) determined a decrease of the number of days of low discharges in winter and an increase in summer in Austria.

So far, climate change impact studies on hydrology in the Austrian Alps using an ensemble of climate projections are limited. However, using simulations of different GCMs and RCMs is essential in order to capture the uncertainty of climate change projections (Addor et al., 2014; Her et al., 2019). To our knowledge, the study by Laghari et al. (2012) implements with 13 the largest number of climate projections, but only investigates impacts on one catchment in Austria. Moreover, to date no study explicitly focuses on study catchments of different elevations in the Alpine region in Austria to assess changes in seasonality and extreme events in runoff. However, a comparison of future changes in catchments based on their altitude is relevant as elevation is a key element influencing hydroclimatic conditions in mountainous areas (Parajka et al., 2009). To investigate future changes on alpine catchments of different altitudes, we compared alpine catchments with different altitude ranges in Austria using an ensemble of climate projections. Our goal was to assess changes in the seasonality of mean runoffs and annual runoff extremes in relation to the altitudes of the catchments at the end of the 21st century.

For this purpose, a semi-distributed hydrological model was customized and calibrated per catchment. Changes between runoff time series in the past and far future were assessed by analyzing changes in timing and magnitude of annual floods and low flows as well as differences in monthly runoff. These changes in runoff are discussed considering altitude differences of the catchments. The study presents changes in the runoff of six alpine catchments for two emission scenarios and an ensemble of 14 climate projections.

2 Methodology

2.1 Study Site and Data

For this study, six catchments with different altitude ranges and hydrological regimes in the Alpine region in Austria were chosen (see Figure 1). Their respective characteristics are shown in Table 1. The Pitztal is the highest catchment with a mean altitude of 2558m and a nivo-glacial regime with 18% glacial coverage. In

Table 2: EURO-CORDEX projections used for this study.

ID	GCM	RCM
1	CNRM-CM5 r1i1p1	CCLM4-8-17
2		ALADIN53
3		RCA4
4	EC-EARTH r1i1p1	RACMO22E
5	EC-EARTH r3i1p1	HIRHAM5
6	EC-EARTH r12i1p1	CCLM4-8-17
7		RCA4
8	CM5A-MR r1i1p1	WRF361H
9		RCA4
10	HadGEM2-ES r1i1p1	CCLM4-8-17
11		RCA4
12		RACMO22E
13	MPI-ESM-LR r1i1p1	CCLM4-8-17
14		RCA4

contrast, the lowest catchment, Feistritztal (917m), has a nivo-pluvial hydrological regime. The other catchments have a nival regime but differ in mean elevation from 1315m (Paltental) to 2233m (Defreggental) with small glacial coverage. Influenced by the differences in altitude, the land cover types of the catchments differ. High elevation catchments consist mainly of bare rock and grassland, whereas more than half of lower elevation catchments is covered by forests (see Table 1).

The location of precipitation, temperature and discharge stations used in this study are also shown in Figure 1. Daily discharge sums were taken from the Hydrographic Service Austria (https://ehyd.gv.at/). Temperature and precipitation data were made available from Austrian Central Institute for Meteorology and Geodynamics (ZAMG) and the Hydrographic Service Austria. Precipitation data was aggregated and temperature data averaged to a daily resolution. The long term water balance of each catchment was computed to check the plausibility of the data. Since the long term precipitation for the Defreggental and Silbertal was lower than long term discharge, the measured discharge was scaled such that the long term water balance matches the Budyko framework. Hereby, it was decided to scale the discharge data rather than the precipitation data, to keep precipitation data of climate projections unchanged.
Land use types of the catchments were determined using the CORINE Land Cover data set from 2018 (https://land.copernicus.eu/pan-european/corine-land-cover) and the riparian zone was determined based on a 10 × 10m height-above-nearest drainage map (HAND) (Prenner et al., 2019). Glacier outlines of the past were taken from the Austrian Glacier Inventory (https://www.uibk.ac.at/acinn/research/ice-and-climate/projects/austrian-glacier-inventory.html.en) (Abermann et al., 2010; Lambrecht & Kuhn, 2007). A linear interpolation between the observation years was applied and the change in glacial area between 1997 and 2006 was extrapolated to 2015. Zekollari et al. (2019) simulate the future evolution of glaciers in Europe with GloGEMflow, a recent extension of a glacier evolution model which considers ice flow explicitly. Results for glaciers in the Pitztal under different emission scenarios are used in this study. They were scaled to match the extrapolated past glacial areas in 2015.
For calibration daily gridded snow cover data from satellites (MOD10A1) was utilized (Hall & Riggs, 2016). Moreover, a 10x10m digital elevation model of Austria (https://www.data.gv.at/katalog/dataset/dgm) was used to derive topographic information. For future temperature and precipitation inputs at the station scale, 14 high-resolution bias corrected climate projections generated based on the EURO-CORDEX data set (see Table 2), each for two emission scenarios – RCP 4.5 and RCP 8.5 – were employed (Switanek et al., 2017). The projections provide data on a daily basis and at the point-scale equal to locations of measurement stations and range from 1950 to 2100.

2.2 Hydrological Model

2.2.1 Model Structure

A process based semi-distributed hydrological model was employed in this research to model the rainfall-runoff behaviour of the catchments. The model is based on a topography-driven approach as utilized and described by Gao et al. (2014) and Prenner et al. (2018). The aim is to represent dominant physical processes in the catchment based on topography and land cover classes while limiting model complexity (Savenije, 2010). Thus, the approach acknowledges the importance of landscape on rainfall-runoff behaviour. The model was adapted to serve the needs of this study and programmed in Julia (https://julialang.org/). All relevant equations are displayed in Table 3, a detailed model description is given in the Appendix A and the code is available on GitHub (https://github.com/sarah-hanus/hbv-mountain). The following processes are included in the model, which are represented by the equations shown in Table 3: interception by vegetation, storage of water as snow, storage of water and evapotranspiration of water in the unsaturated zone as well as a fast and slow responding component, i.e. groundwater. In total, the model has three levels of spatial resolution which are, in ascending resolution, the precipitation zones, the hydrological response units (HRUs) and the elevation zones.

Figure 1 shows the division of catchments into precipitation zones based on available precipitation gauges using Thiessen polygons. The model is run separately for each precipitation zone with different precipitation input. Model outputs are summed according to the areal weights. Figure 2 shows a schematization of the model structure. The model, run for each precipitation zone separately, is divided into four HRUs: bare rock, forest, grassland and riparian zone. These classes differ in vegetation. Thus, the interception and soil stor-

Table 3: Equations implemented in the hydrological model, $area_{gl}$: glaciated area. A more detailed description can be found in Appendix A

Reservoir	Water balance equation	Constitutive functions
Interception	$\frac{dS_{int}}{dt} = P_{rain} - E_{int} - P_{eff}$	$P_{eff} = max(S_{int} - I_{max}, 0)$ $E_{int} = min(0.5 \cdot E_{pot}, S_{int})$
Snow	$\frac{dS_{snow}}{dt} = P_{snow} - M_{snow}$	$M = F_{melt} \cdot M_M(\frac{T-T_{thresh}}{M_M} + ln(1 + \exp(-\frac{T-T_{thresh}}{M_M}))$ $M_{snow} = min(M, S_{snow})$ $M_{glacier} = M$ $M_{tot} = M_{snow} \cdot (1 - area_{gl}) + M_{glacier} \cdot area_{gl}$
		$P_{eff,tot} = \sum_{i=1}^{Elevations} P_{eff} + \sum_{i=1}^{Elevations} M_{tot}$
Unsaturated Zone	$\frac{dS_{soil}}{dt} = q_{soil} - E_{soil}$	$C_r = 1 - (1 - \frac{S_{soil}}{S_{soil,max}})^{\beta}$ $q_{soil} = min((1 - C_r) \cdot P_{eff,tot}, S_{soil,max} - S_{soil})$ $q_{soil,rip} = min((1 - C_r) \cdot (P_{eff,tot} + q_{rip}), S_{soil,max} - S_{soil})$ $S_{soil} = S_{soil} + q_{soil}$ $E_{soil} = (E_{pot} - E_{int}) \cdot min(\frac{S_{soil}}{S_{soil,max} \cdot F_{evap}}, 1)$
Fast Reservoir	$\frac{dS_{fast}}{dt} = q_{overland} - q_{fast}$	$q_{overland} = (P_{eff,tot} - q_{soil}) \cdot \rho_p$ $q_{overland,rip} = P_{eff,tot} + q_{rip} - q_{soil,rip}$ $q_{fast} = k_{fast} \cdot S_{fast}$
Slow Reservoir	$\frac{dS_{slow}}{dt} = \sum_{i=1}^{HRU} q_{pref} - q_{slow}$	$q_{pref} = (P_{eff,tot} - q_{soil}) \cdot (1 - \rho_p)$ $q_{slow} = k_{slow} \cdot S_{slow}$

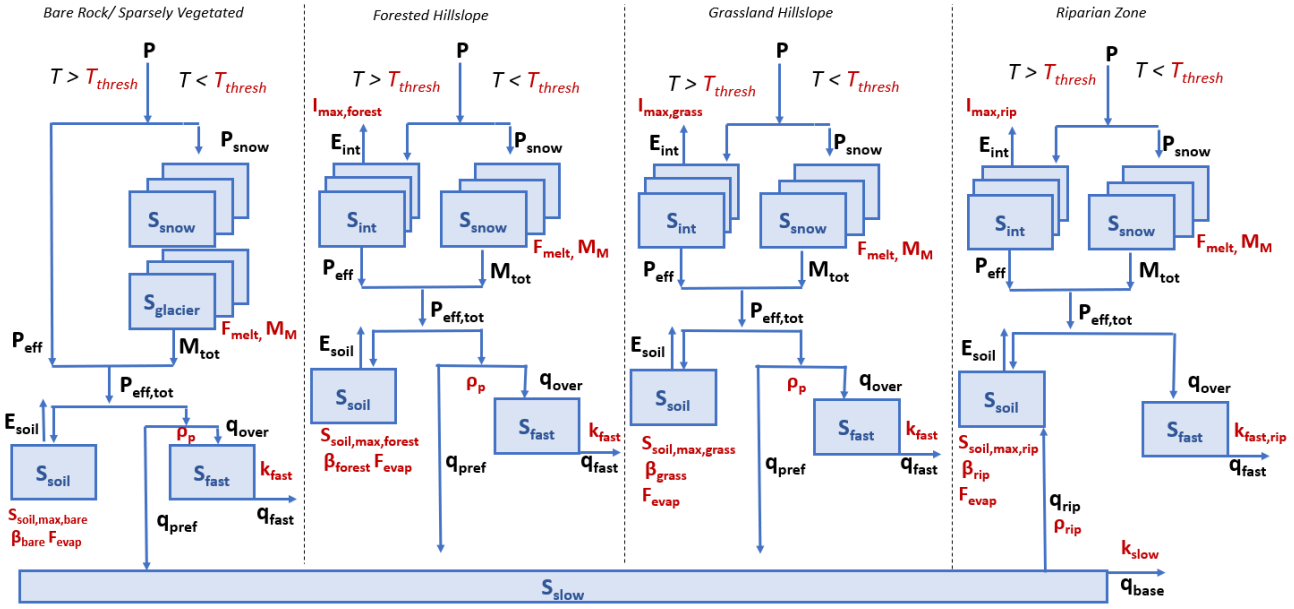

Figure 2: Schematization of model structure per precipitation zone, blue represents states, black fluxes and red parameters. **Parameters**: β: factor accounting for nonlinearity, F_{evap}: evapotranspiration control factor, F_{melt}: melt factor, I_{max}: max. interception capacity, k_{fast}: fast hillslope constant, $k_{fast,rip}$: fast riparian constant, k_{slow}: slow constant, M_M: smoothness parameter for melt, ρ_p: share preferential flow, ρ_{rip}: share riparian flow, $S_{soil,max}$: max. soil storage capacity, T_{thresh}: threshold temperature. **Reservoirs/States**: S_{fast}: fast responding reservoir, $S_{glacier}$: glacier reservoir, S_{int}: interception reservoir, S_{slow}: slow responding reservoir, , S_{snow}: snow reservoir, S_{soil}: soil reservoir. **Fluxes**:E_{int}: interception evaporation, E_{soil}: evapotranspiration, M_{tot}: melt, P: precipitation, P_{snow}: precipitation as snow, $P_{eff,(tot)}$: (total) effective precipitation, q_{base}: base flow, q_{fast}: fast runoff, q_{over}: overland flow, q_{pref}: preferential flow, q_{rip}: capillary rise riparian zone.

age characteristics of the land use classes are expected to differ, which is represented in the model by varying these parameters between HRUs. Other parameters are kept constant across HRUs to minimize calibration parameters. Also, process representations slightly differ per HRU based on the process understanding of the landscape class. For example, interception is not considered in the bare rock class since it is expected

to be negligible due to at most sparse vegetation cover. The riparian zone includes the process of capillary rise of water to the soil due to low groundwater tables. Glaciers are incorporated in the model as an unlimited snow reservoir in the bare rock unit (Mostbauer et al., 2018; Seibert & Vis, 2012). The HRUs are run separately and the total runoff generated each time step is calculated as the weighted sum of the runoffs generated by the fast responding components of the individual units and the slow responding component which spans all hillslope HRUs.

Partitioning of precipitation into rain and snow is temperature and therefore altitude dependent. To obtain a more realistic representation of this process, catchments were divided into elevation zones of 200m altitude, for which this process, as well as interception, snow storage and melt, was modelled individually. Melt is calculated with an improved degree-day method as suggested by Girons Lopez et al. (2020).

In addition to temperature and precipitation, potential evaporation is needed as input for the hydrological model. The latter was calculated based on daily temperature and potential sunshine hours using the Thornthwhaite method (Oudin et al., 2005; Thornthwaite, 1948).

2.2.2 Calibration & Evaluation

In total 20 parameters had to be calibrated for each catchment, except for the Pitztal, where a loss term had to be implemented due to divergence of water from the catchment, resulting in an additional parameter. All model parameters were constrained a priori based on literature (Prenner et al., 2019; Gao et al., 2014) (see Appendix B). The parameter combinations of HRUs were constrained based on Gharari et al. (2014), e.g. the interception capacity of forest has to be larger than for grassland (see Appendix B).

For a robust calibration, multiple objective functions are used. This approach has been applied in numerous studies to ensure correct process representation by the model (Efstratiadis & Koutsoyiannis, 2010). In this study eight objective functions were used which cover the timing of high and low flows, the magnitude of flows, the memory of the catchment and the partitioning between runoff and evaporation (see Table 4). The overall performance was assessed by the mean Euclidean distance (D_E) from the perfect model fit, e.g. Hrachowitz et al. (2014). The objective functions were weighted equally because the calibrated model should be able to reproduce the overall system dynamics.

For model calibration, Monte Carlo sampling with 3.000.000 realizations was employed for each catchment. Calibration was run for a period of 20 years (Oct. 1985- Oct. 2005) with a warm-up period of three years. Excluding disinformation from the calibration process by removing incorrect input data improves the validity of the model predictions due to improved system representation (Beven & Westerberg, 2011). Therefore, in a second run four events with major data inconsistencies were omitted during calibration of each catchment. The decision on which events to omit was based on visual inspection of the hydrographs in comparison to the precipitation. Events with observed discharge peaks without a prior peak in rainfall outside the snow melt season were excluded, as well as major events where the peak in observed runoff exceeded the peak in modelled runoff by more than 100%.

The calibration was evaluated using a period of 8 or 10 years depending on data availability from 2005 to 2013 (2015). For the evaluation of the model performance, the same objective functions as for calibration were used. To partially capture the model uncertainty but still limit the the amount of data for further analysis, the best 0.01% of the calibrated parameter sets (approx. 300 sets) were used for further analysis with the additional criterion of an Euclidean distance below 0.2 during calibration. This decision is based on the concept of equifinality, suggesting that observed runoff behaviour can be acceptably reproduced by many different parameter sets (Beven & Binley, 1992). Subsequently, these parameter sets are called best parameter sets. To fully represent model uncertainty is beyond the scope of this work.

2.3 Climate Projections

Seasonality in precipitation and temperature of climate projections and observed station data were compared for a 30 year time period in the past to ensure that the climate projections show a similar seasonality as observations in the past. Moreover, climate projections were used as model input to model the runoff behaviour in the past. The projections should match the probability distributions of the real runoff data but not the runoffs at a specific time. Therefore, the modelled mean monthly runoff and the timing and magnitude of maximum and minimum annual runoffs were compared to measured discharge in the past.

After checking the climate projection data of the past, the best parameter sets were fed into the model together with the climate data of the climate projections to model the catchment behaviour for a 30 year time period in the past (1981-2010) and at the end of the 21st century (2071-2100). In total, 14 times 300 simulations were performed per catchment and emission scenario. The HRUs are kept constant for all time periods, whereas the glacier area of the Pitztal is subject to change. The glacier area of the Defreggental was assumed zero for the future time period. The results were utilized for change analysis of runoff patterns in the future.

2.4 Analysis of Change

To analyse future changes in runoff behaviour, the simulations of the past and future using the same climate projection and parameter set were compared. For the Pitztal, the loss term was omitted for further analysis

Table 4: Signatures & objective functions, as objective functions the Nash Sutcliffe Efficiency NSE, the volumetric error (VE) and the relative and absolute error (RE, AE) are used.

Signature	Abbreviation	Objective Function	Reference
Timeseries of Flow	Q	$E_{NSE,Q}$	(Nash & Sutcliffe, 1970)
		$E_{NSE,log(Q)}$	(Nash & Sutcliffe, 1970)
		$E_{VE,Q}$	(Criss & Winston, 2008)
Flow Duration Curve	FDC	$E_{NSE,FDC}$	(Euser et al., 2013)
Autocorrelation	AC1	$E_{RE,AC1}$	(Euser et al., 2013)
	AC90	$E_{NSE,AC90}$	
Monthly Runoff Coefficient	RC	$E_{NSE,RC}$	
Snow Cover	SC	$E_{AE,SC}$	(Finger et al., 2015)

in the past and future period. Generally, averages over the 30 year time period are used to get a robust comparison and decrease noise of yearly fluctuations. To better understand shifts in runoff patterns, the relative and absolute changes of 30 year average monthly discharge volumes as well as monthly melt volumes were computed per model simulation. For investigating total water availability, the changes in average annual discharges were also computed. The methodology for analysing changes in extremes – high flows and low flows – is described in the following paragraphs, equations are given in Appendix C.

2.4.1 High Flows

For investigating the changes in high flows, a similar approach to Blöschl et al. (2017, 2019) was taken. A series of discharges consisting of the highest peak flow modeled for each calendar year – the annual maximum flow (AMF) – was used. For analysing the change in magnitudes of high flows, the relative and absolute changes in average AMF magnitude were examined for each simulation. Moreover, the magnitudes were ranked and the exceedance probability was calculated. The absolute changes in magnitude for a certain return period, related to an exceedance probability, were calculated per simulation. This approach allows a more detailed investigation of magnitudes of AMF. For computing the mean timing of high flows over the time period, the method of circular statistics was used (e.g. Blöschl et al. (2017); Young et al. (2000)). This method computes time differences between events correctly despite turns of the year. Nevertheless, a bimodal flood season would be hidden by this approach, as the average date of occurrence would be located between the two seasons. Therefore, not only the average timing of occurrence was compared, but also the distribution of timing in the 30 year period was analyzed. Hence, the fraction of incidences over all years within 15 day periods was computed. A 15 day period was chosen to allow observations of small changes. However, the time span is still large enough for multiple events to co-occur in the same period. This approach allows a more detailed representation of shifts in timing of AMF.

2.4.2 Low Flows

Changes in low flows were analysed using two approaches. First, the yearly minimum average discharge of 7 consecutive days using a moving average was computed from June to May to avoid complications with turns of the year as low flows are expected mainly in winter (Jenicek et al., 2018; Vormoor et al., 2017). The average magnitude and timing were determined for the period and the distribution of timing over the 30 year period was analyzed according to the approach taken for high flows. Second, a threshold approach was used to identify days of low flows. As threshold the Q_{90}, the magnitude of flow which is exceeded in 90% of the time during the simulation of the past, is used (Blahušiaková et al., 2020). The average monthly number of days below this threshold and the corresponding monthly deficit volume were determined. The monthly deficit volume gives an indication of the severity of low flows. It is defined by how much water is missing each month in order to reach the threshold runoff (Q_{90}) during all days of the month.

3 Results

3.1 Calibration & Evaluation

The calibration and evaluation results show a good representation of the runoff dynamics by the model with the mean Euclidean distance (D_e) ranging from 0.11 to 0.18 from the perfect model fit during calibration and 0.11 to 0.20 for the evaluation period as shown in Figure 3. Nevertheless, an increase in D_e with decreasing mean elevation of the catchment can be observed, as a result of decreased performance of NSE and NSElog. This phenomenon can be explained by a strong seasonality in high altitude catchments compared to more flashy discharge patterns in lower altitude catchments. The Silbertal shows the strongest decrease in performance during the evaluation period ($D_{e,cal}$=0.12 and $D_{e,eval}$=0.2), whereas for the other catchments performance remains comparable. A visual inspection of the hydrographs reveals that timing of modelled and observed runoff and magnitudes of low flows match well. However, magnitudes of peak runoffs are mostly underestimated by the model. A possible reason can be that

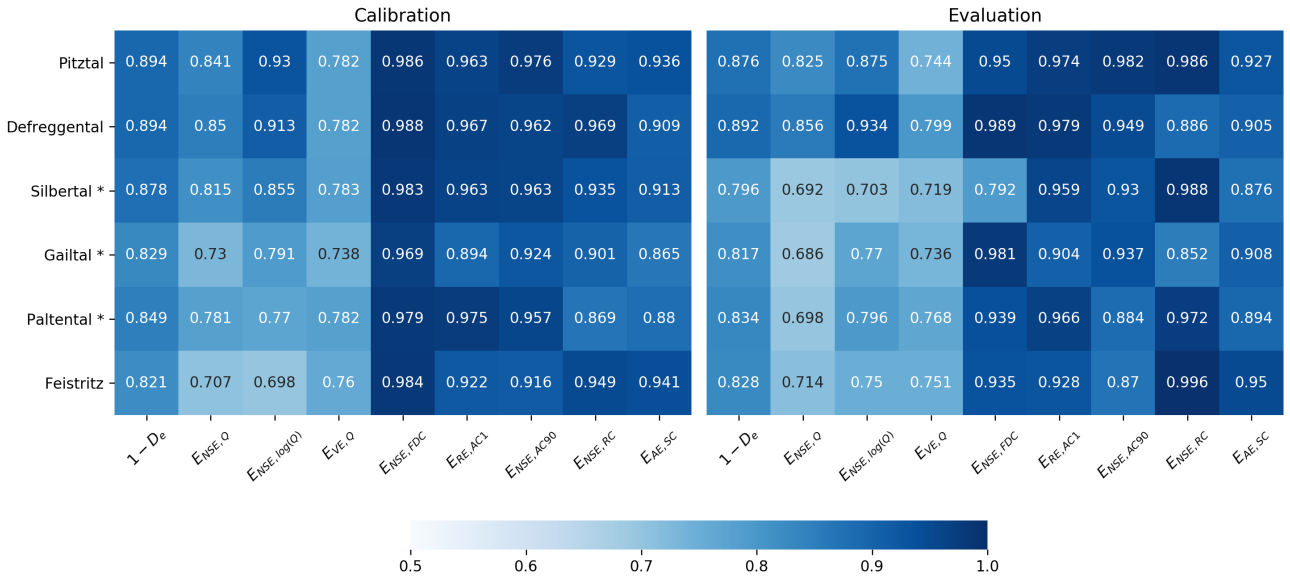

Figure 3: Mean calibration and evaluation results of 300 best parameter sets. $1 - D_e$ shows the overall model fit, D_e denotes the mean Euclidean Distance from the perfect fit, * indicates 8 years of evaluation instead of 10 years. The calibration excludes time periods of disinformation.

precipitation amounts recorded at precipitation gauges during heavy precipitation does not match the actual precipitation over the whole area. Example plots of modelled and observed hydrographs can be found in Appendix D.

3.2 Climate Projections

The seasonality of precipitation and temperature of climate projections in the past matches the seasonality of the measured station data, only few differences were observed. For the higher elevation catchments (Silbertal, Defreggental, Pitztal), the projections underestimate the monthly temperatures, mostly in the summer months. Overview figures for each catchment can be found in Appendix E. The seasonality in monthly discharge is generally well represented by the modelled runoff using climate projections. However, monthly discharge is overestimated for all months in the Feistritztal. Moreover, runoff is underestimated in April and May in the Paltental. In high elevation catchments it can be observed that monthly runoff, generated using climate projections, is underestimated in spring and early summer, whereas it is overestimated in late summer. This is probably due to the underestimation of temperature in these catchments by climate projections.

Regarding annual extreme events, the distribution of timing of annual maximum precipitation, annual maximum runoff as well as annual minimum runoff of the measured data and the climate projections match. Only in the Feistritztal and Pitztal model results using climate projections indicate an earlier timing of minimum annual runoff than measured data. Concerning the magnitudes of annual extremes, precipitation and minimum runoff magnitudes of measured data and model results using climate projections match well, underestimated minimum runoffs by the model results in the Pitztal mark an exception. However, magnitudes of annual maximum runoffs are underestimated by model results for all catchments. This can be related to the aforementioned underestimation of magnitudes of peak runoffs by the calibrated model.

3.3 Hydroclimatic Change

Firstly, the changes in average annual precipitation, temperature and discharge between the past 30 year period and the far future were analysed (Figure 4). The increase in temperature is similar across catchments, with a median increase across climate projections of 2-3°C for RCP 4.5 and 4-5°C for RCP 8.5. The median increase is largest for the Defreggental and Pitztal. On average climate projections show an increase of annual precipitation by 4% (RCP 8.5 Gailtal) to 9% (RCP 8.5 Defreggental). The median absolute change ranges from 50mm/yr to 100mm/yr across catchments. However, the spread between climate projections is large, with one projection suggesting a decrease of 10% or larger for all catchments and another an increase of more than 20% for the Defreggental (+180mm/yr) and Pitztal (+185mm/yr). Generally, a decrease in precipitation is projected for July and August for most catchments, while an increase in precipitation is projected for the rest of the year (see Figure F).

For RCP 4.5 the annual discharge increases by around 5%, which translates into an absolute change from 18mm/yr for the Feistritztal up to 56mm/yr for the Silbertal. For the Pitztal an increase of 12% (50mm/yr) was modelled. For RCP 8.5 the median change is around zero for the Feistritztal, Paltental and Gailtal. However, the spread between simulations is

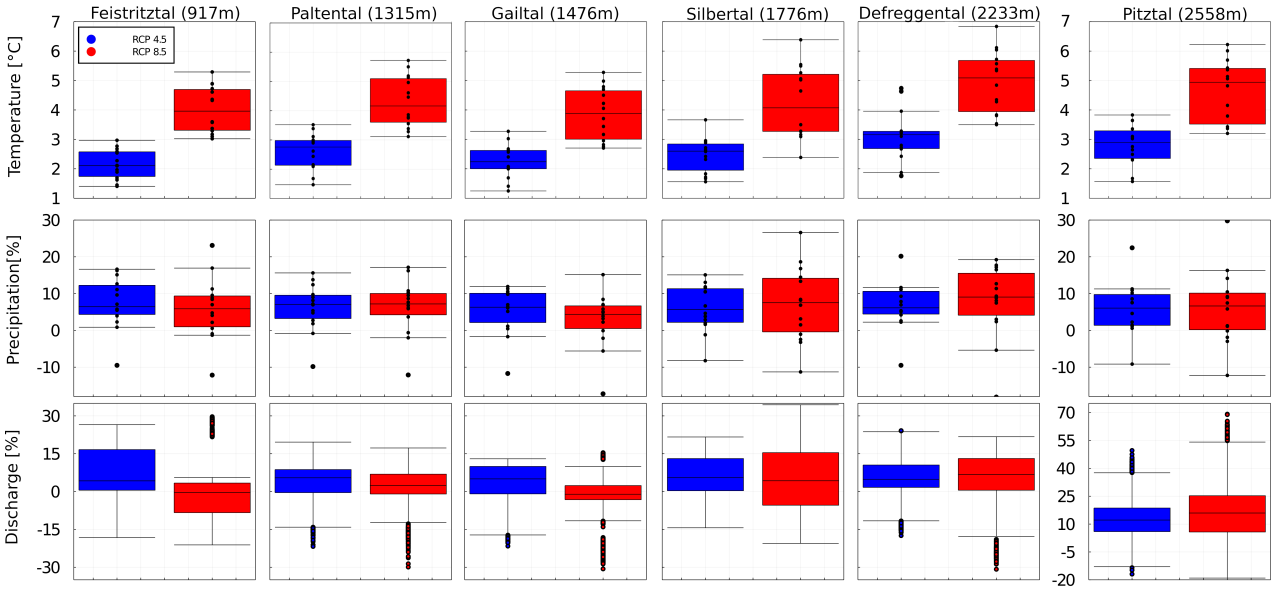

Figure 4: Boxplots showing absolute changes in mean annual temperature and relative changes in mean annual precipitation of the 14 climate projections (black dots representing the individual climate projections), relative change in annual discharge of all simulations.

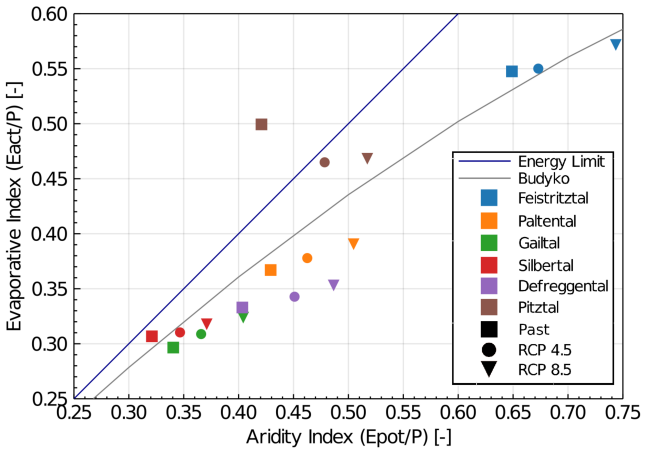

Figure 5: The mean location of the study catchments in the Budyko framework in the past and under two emission scenarios at the end of the 21st century.

large. For the Defreggental and Pitztal the median increase in discharge is +7% (42mm/yr) and +15% (69mm/yr) and thus larger for RCP 8.5 compared to RCP 4.5. Hence, the change in annual discharge is larger for higher elevation catchments under RCP 8.5.

Moreover, the mean position of the catchments in the Budyko framework are displayed in Figure 5, which gives an overview of the changes in hydroclimatic conditions in future. All catchments but the Pitztal move to the top right in the Budyko framework, which means that the aridity as well as the evaporative index increase. The aridity index increases stronger. This implies that more energy is available for evaporation in future and therefore evaporation increases. Thus, the runoff coefficient decreases in future by 0.0025-0.012 under RCP 4.5 and 0.011-0.027 under RCP 8.5. The change is around twice as large for RCP 8.5 compared to RCP 4.5. The Pitztal plots outside the energy limit in the past using data of climate projections, suggesting too little runoff as the evaporative index is calculated indirectly by $1 - \frac{Q}{P}$.

3.4 Hydrological Change

Figure 6 shows exemplary hydrographs to illustrate hydrological changes. A shift towards an earlier increase of runoff can be seen for the Defreggental, whereas changes are less clear for the Feistritztal. In the following, the hydrological changes, extracted by statistical methods over all simulations, are presented.

Looking at the change in seasonal runoff coefficients of the catchments reveals substantial differences between the lower elevation catchments (Feistritztal, Paltental, Gailtal) and the higher elevation catchments. For the higher elevation catchments a median increase in runoff coefficients is observed in spring (0.1-0.5) and to a lesser extend in winter (0.03-0.1) (see Figure 7). The lower elevation catchments show a median decrease in seasonal runoff coefficient in spring (-0.03 to -0.1) but an increase in winter (0.05-0.15). Only under RCP 8.5 the Feistritztal displays a decrease of 0.1 in winter runoff coefficient. In summer and autumn, a decrease in seasonal runoff coefficient is observed for the lower elevation catchments with exception of Feistritztal under RCP 4.5. For the higher elevation catchments, the decrease in seasonal runoff coefficient is larger in summer ranging from 0.1 to 0.3, whereas the runoff coefficient in autumn only show minor changes.

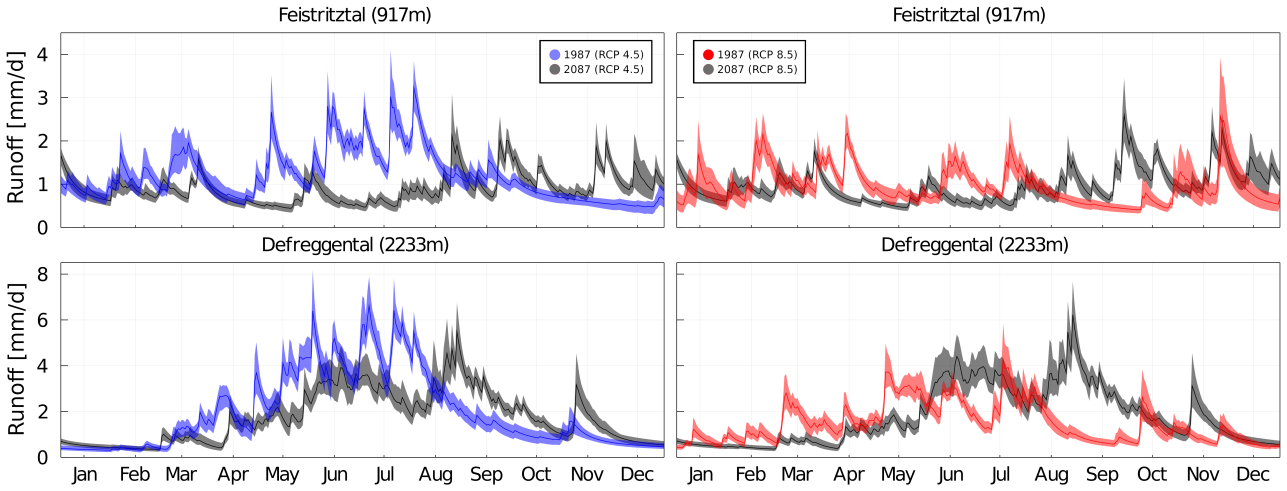

Figure 6: Runoff in past and future of lower and higher elevation catchments illustrated by hydrographs of 1987 and 2087 under RCP 4.5 and RCP 8.5 for the Feistritztal and Defreggental for Projection-14. The shaded area is the range of runoffs modelled by the best parameter sets, the line the mean. An overview figure for all catchments can be found in Appendix F

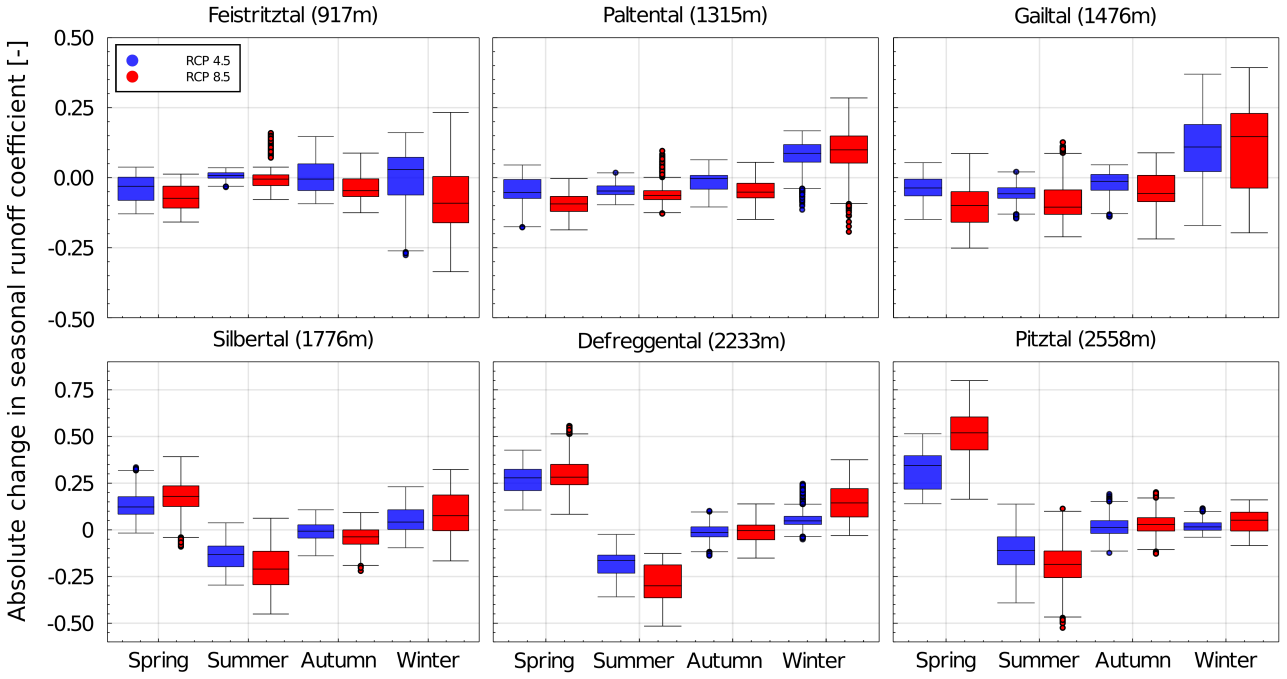

Figure 7: Absolute changes in mean seasonal runoff coefficient, spring: Mar-May, summer: Jun-Aug, autumn: Sep-Nov, winter: Dec-Feb; mean elevation in brackets.

3.4.1 Monthly Discharges

The mean monthly discharge increases at the end of the century in winter and spring months (25-100% for RCP 4.5) and decreases in summer months (10-20% for RCP 4.5) as shown in Figure 8 & F. Changes are up to twice as large for RCP 8.5 compared to RCP 4.5 and also the spread between simulations is larger. The Feistritztal is an exception with a positive change in summer discharges for RCP 4.5 of 0.2mm/d. Moreover, it shows a similar increase in winter discharge for both emission scenarios of 0.2mm/d as seen in Figure 8.

Looking at the timing of changes reveals that the largest relative and absolute increase in discharge occurs later for catchments with higher mean altitude. For the Gailtal the largest absolute increase occurs in February (0.6-0.8mm/d), for the Silbertal (0.8-1.2mm/d) and Defreggental (0.8-1.0mm/d) it occurs in April and for the Pitztal in May with an increase of 1 to 1.4mm/d. The Feistritztal and Paltental do not show a distinctive month with largest increase. Figure 8 also indicates that a decrease in monthly discharge already occurs in May for Feistritztal, Paltental and Gailtal, whereas for the Silbertal and Defreggental it occurs in June and in the Pitztal lower discharges are

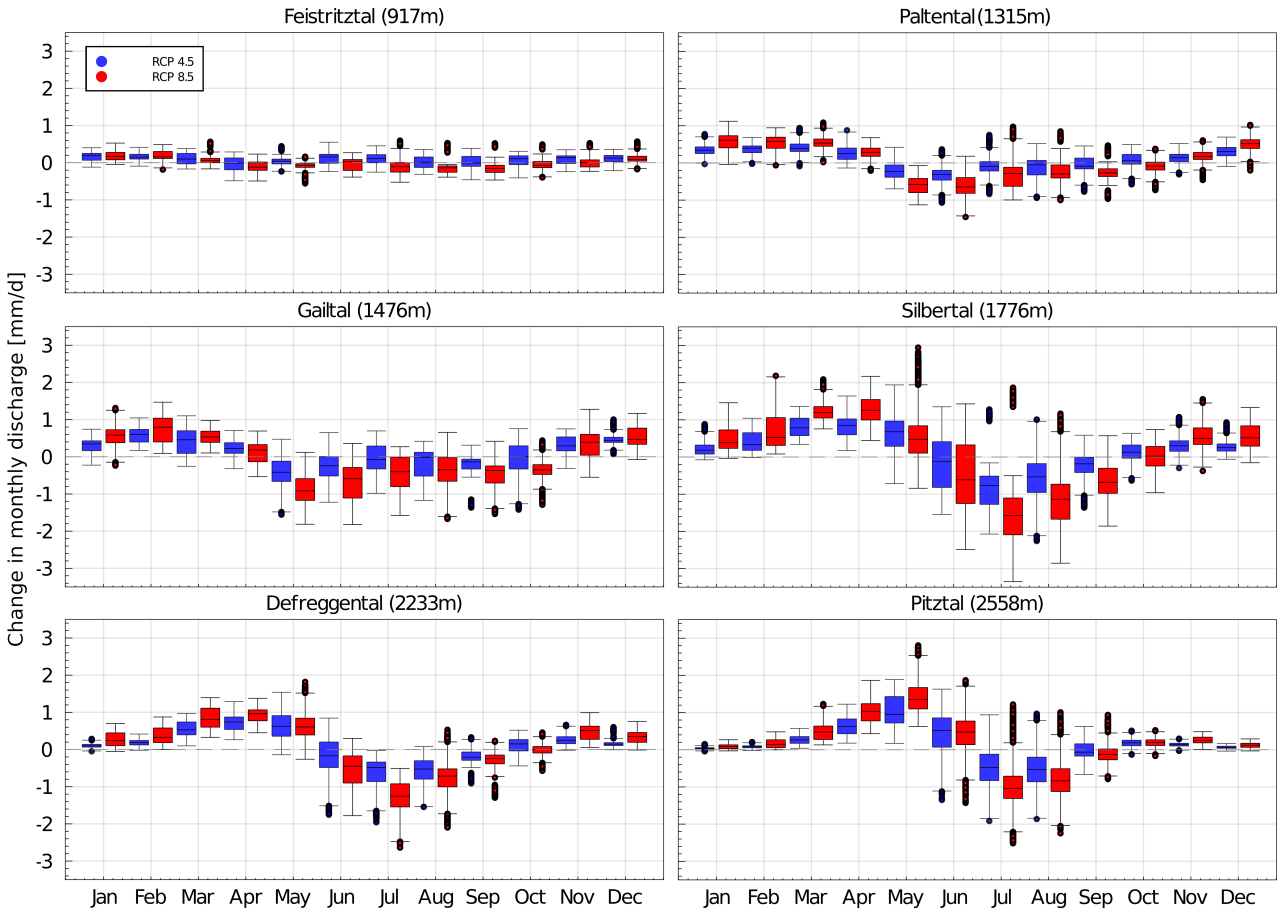

Figure 8: Absolute changes in mean monthly discharge of all catchments, mean elevation in brackets.

only modelled for July to September. The largest decrease of monthly discharge in summer occurs in August/September for the Feistritztal, in June for the Paltental, in May for the Gailtal and in July for the higher elevation catchments.

Moreover, the results imply that the absolute change in monthly discharge generally increases with increasing mean catchment elevation. The change is very limited for the Feistritztal (± 0.2mm/d), larger for the Gailtal (± 0.9mm/d), while the absolute decrease in discharge is largest for the Silbertal (-1.5mm/d RCP 8.5) and the absolute increase in discharge is largest for the Pitztal (1.5mm/d RCP 8.5). However, looking at relative changes, the decrease in the Silbertal is similar to the decrease in the Defreggental and Pitztal (around 25%). Relatively, the increase in spring discharge is largest for the Pitztal (100-200% median increase in March), followed by the Defreggental with a median increase of 100-150% in March (see Figure F). The underlying reason is lower discharges in winter months in these catchments compared to catchments with lower mean altitude.

3.4.2 Timing of High Flows

A substantial shift in timing of annual maximum flows (AMF) is observed towards the end of the 21st century ranging from -9 to -31 days for high elevation catchments and +4 to -17 days for lower elevation catchments. The Gailtal is the only catchment exhibiting a substantial shift towards later occurrences in AMF (see Table 5). As shown in Table 5, the average timing of AMF for the past period is beginning of July for the higher catchments and beginning of June for the lower catchments (Feistritztal, Paltental). In the Gailtal the AMF occurs on average beginning of October. The higher catchments show a shift of -11 to -20 days on average for RCP 4.5 with the Silbertal exhibiting the largest shift of -20 days. For RCP 8.5 the Defreggental shows a similar shift as for RCP 4.5, whereas the Silbertal and Pitztal show an increased shift of -31 and -22 days. The lowest catchments only exhibit a minor change in mean timing of AMF for RCP 4.5 and an average shift forward of half a month for RCP 8.5. The greatest change is observed for the Gailtal with a model mean shift of +29 days for RCP 4.5 and +48 days for RCP 8.5. For all catchments but the Gailtal, the standard deviation increases in future with larger increases for RCP 8.5.

However, mean timing might hide bimodal distributions in timing of AMF. Analysing the fraction of timing of occurrence within the 30 year time period gives additional information about the intensity of seasonality (Figure 9). It reveals a bimodal AMF seasonality for the

Table 5: Mean and standard deviation of timing of AMF across all simulations, based on the average timing of AMF over 30 years of each simulation, dates shown as day of year, for the past the date is given as reference.

	Past	Date	RCP 4.5	RCP 8.5	Change RCP 4.5	Change RCP 8.5
Feistritztal	159±12	8th of June	163±19	142±36	+4 days	-17 days
Paltental	165±9	14th of June	163±17	151±23	-2 days	-14 days
Gailtal	277±25	4th of October	306±22	325±21	+29 days	+48 days
Silbertal	186±8	5th of July	166±12	155±17	-20 days	-31 days
Defreggental	188±9	7th of July	177±13	179±17	-11 days	-9 days
Pitztal	185±7	4th of July	171±11	163±15	-14 days	-22 days

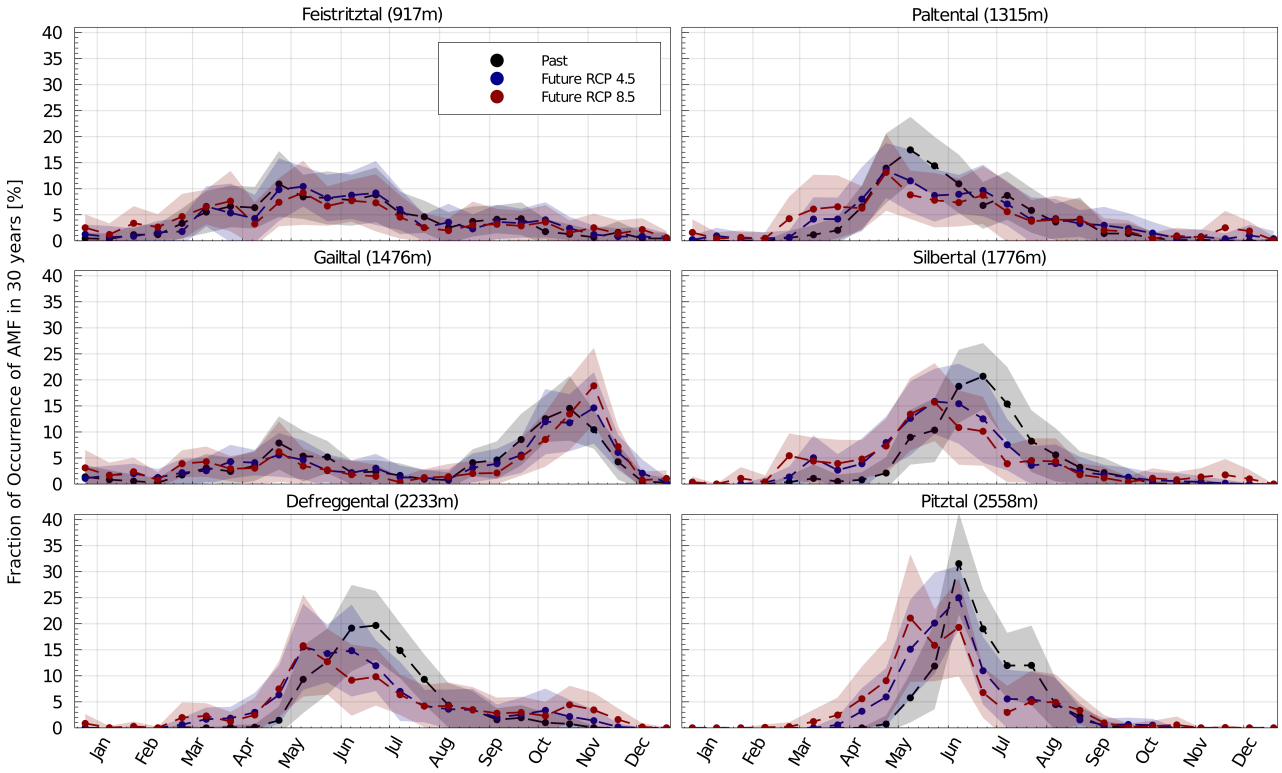

Figure 9: Simulation mean fraction of occurrences of AMF in 30 years using time windows of 15 days, uncertainty band of 1 std is shaded. Dashed lines between 15 day periods are used for better visualization.

Gailtal, with AMF occurring in beginning of May and beginning of October. A relationship between mean elevation of the catchment and timing and seasonality of AMF can be observed for the past. For the lowest catchment (Feistritztal) AMF occurrences are widely spread over the year with most incidents beginning of May. The Paltental shows most incidents end of May, whereas the high elevation catchments exhibit most AMFs in June and July and have the highest seasonality. A clear shift towards earlier occurrences of annual maximum flows can be distinguished for catchments with a high mean elevation. However, also the Paltental shows a substantial increase in AMF events in March for RCP 8.5. The seasonality in timing of AMF is less pronounced in future. Thus, the potential flood season expands in future, on average by around half a month to a month for the Paltental. In the Silbertal the potential flood season extends on average by 1-3 months, in Defreggental by 2-3 months and in the Pitztal by 1-1.5 months. Comparing the results of RCP 4.5 with the results of RCP 8.5 reveals that changes are more pronounced for the higher emission scenario and timing of AMF is more spread out over the year for RCP 8.5.

3.4.3 Magnitude of High Flows

The model median average magnitude of AMF over 30 years increases for all catchments under RCP 4.5 by around 10%, except for the Paltental which shows only an increase of 2% and the Pitztal which shows an increase of 18% (see Figure 10). The absolute change is largest for the Gailtal (1.4mm/d), followed by the Pitztal (1.1mm/d). The average AMF magnitude shows a lower increase for RCP 8.5, or even a decrease in case of the Paltental. Only for the Gailtal and Pitztal the relative and absolute increase in mean AMF is slightly larger for RCP 8.5 compared to RCP 4.5, 1.6mm/d and 1.2mm/d respectively. However, the ranges of change and thus the uncertainties are large, especially for the Paltental, Silbertal and Defreggental, where simula-

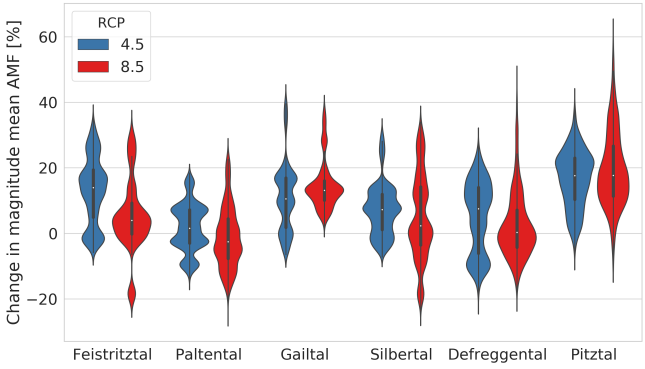

Figure 10: Violin plots of relative change of magnitude of AMF across simulations based on average magnitude over 30 year time period of each simulation.

tions also indicate a decrease in magnitude of AMF in future.

Figure 11 displays a more detailed analysis of magnitudes of AMF in relation to the return periods. It reveals a larger absolute increase in magnitude of AMF for higher return periods but also increasing uncertainty. The standard deviation of a return period of one year is 0.5 to 2mm/d, whereas it reaches 1.7- 9mm/d for a return period of 30 years. A similar pattern can be observed for relative changes. The largest increase in magnitude of AMF at high return periods is exhibited by the Gailtal for RCP 8.5 with an increase of around 8mm/d (+40%). The second largest increase is observed in the Pitztal with 3mm/d (+32%) for both emission scenarios. The two other high elevation catchments display a change of around 2mm/d for RCP 8.5 and 1mm/d for RCP 4.5. The two lower elevation catchments, Feistritztal and Paltental, only show a small increase of 0.6mm/d and 1.0mm/d respectively. For low return periods Paltental and Defreggental show a slight decrease in simulation mean magnitude of AMF for RCP 8.5. The Feistritztal and Silbertal show a larger change for RCP 4.5 than RCP 8.5 for return periods lower than 20 years.

3.4.4 Low Flows

As expected the lowest flows in the year occur most often during the winter months in the past. For the lower catchments, the fraction of occurrence of lowest flows in winter months decreases significantly in future as shown in Figure 12. Especially for RCP 8.5 lowest flows tend to occur more often in early autumn with 13% of annual minimum flows occurring in late September for Paltental and Gailtal. In the Feistritztal, no clear seasonality in occurrence of minimum flows is distinguishable for the far future. In the higher catchments, annual minimum flows occur in the past in late February to March. These occurrences shift towards January and February in future.

Looking at the magnitude of the lowest flows in a year shows a remarkable increase of 12-50% in the higher elevation catchments with significantly larger increase for RCP 8.5 as visible in Figure 13. The Defreggental shows the largest relative change with a median increase of 30% for RCP 4.5 and 50% (+0.47mm/d) for RCP 8.5. The second largest increase is observed in the Pitztal with a simulation median increase of 27% for RCP 4.5 and 40% (+0.11mm/d) for RCP 8.5. Regarding the lower elevation catchments, the Paltental shows an increase in magnitude of minimum flows of 20% (+0.7mm/d) for both emission scenarios. The median increase in magnitude for the Feistritztal and Gailtal is below 10% for RCP 4.5 and zero for RCP 8.5. The absolute changes are largest for Paltental (+0.7mm/d), followed by Defreggental under RCP 8.5 (+0.47mm/d) and Gailtal under RCP 4.5 (+0.35mm/d). To exclude the influence of changes in precipitation on low flows, the change in ratio of Q_{90} (discharge exceeded 90% of the time) and precipitation was analysed as shown in Figure 13 in the lower row. The differences between emission scenarios and catchments is similar to the change in magnitude of minimum yearly flows. However, the relative increase is lower for all catchments. Feistritztal and Gailtal even show a median decrease of the Q_{90} precipitation ratio for RCP 8.5 of -4% and -5%. Regarding the uncertainty, the violin plot reveals that the increase in minimum flow is evident for the higher elevation catchments, whereas the sign of change is more uncertain for the lower elevation catchments, especially Feistritztal and Gailtal.

To examine the severity of low flows in future, the monthly deficit in flow based on Q_{90} as threshold for the past and future was determined (Figure 14). The larger the value of the monthly deficit, the more severe the low flows. A monthly deficit of zero implies that runoff is above the Q_{90} threshold during the whole month. It can be clearly seen that the seasonality in deficit depends on the altitude of the catchment. The Silbertal, Defreggental and Pitztal show almost no deficit from May to November, which does not change in future. In the lower elevation catchments deficits in discharge occur in more months with the Feistritztal exhibiting deficits in all months. The monthly deficit decreases considerably during the winter months in future, especially for RCP 8.5, with largest median decreases of 0.9mm/d in Silbertal followed by the Defreggental with 0.7mm/d. In the Feistritztal and Paltental, a decrease in deficits occurs from October to March (November to March) for RCP 4.5, whereas for RCP 8.5 it only occurs from December to March. For both emission scenarios, the deficit decreases for Gailtal and Silbertal from December to March and for Defreggental from January to April. This illustrates that decreases in deficit shift to later months with increasing mean elevation of the catchments. Moreover, the lower elevation catchments show an increase of deficit in future during the summer and early autumn, especially for RCP 8.5. In Feistritztal the increase in deficit reaches from July to October, in the Paltental from September to October and in Gail-

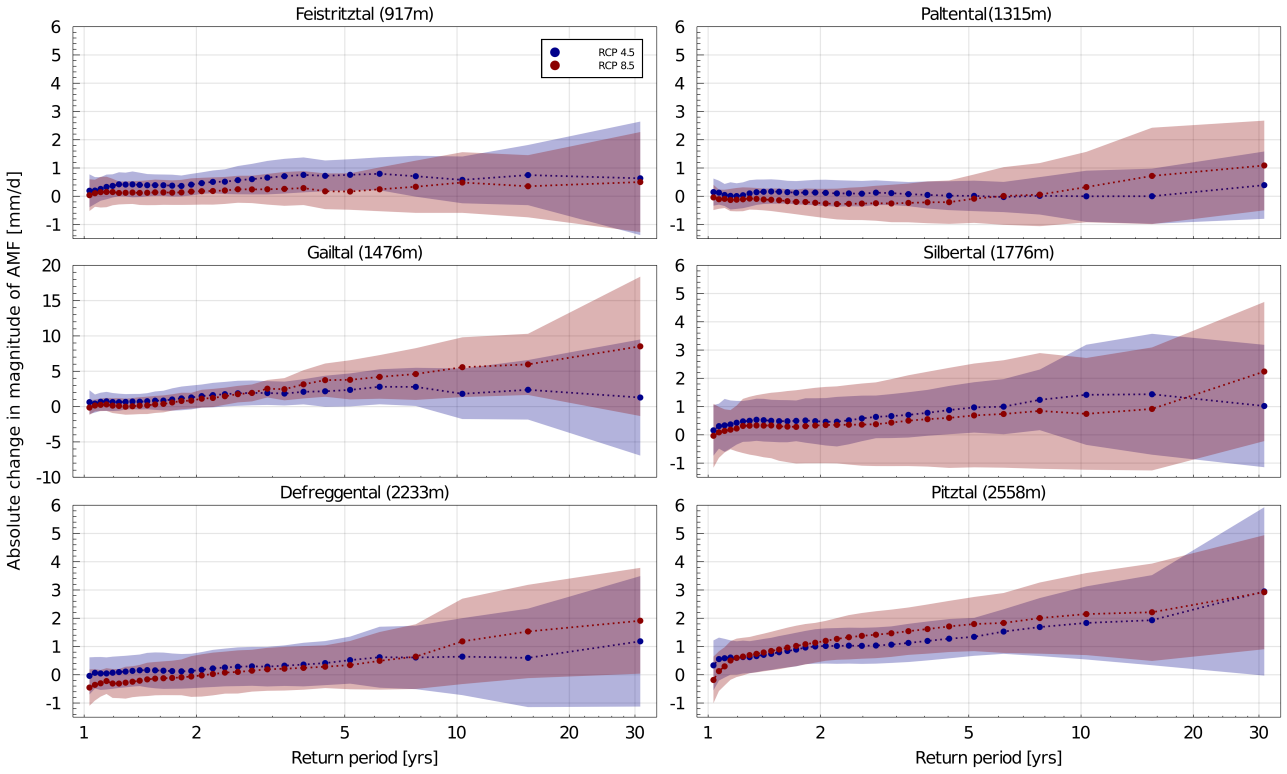

Figure 11: Simulation mean absolute change in magnitudes of AMF in relation to the return period, shaded area indicates 1 std, dotted lines are used for better visualization. Note the different scale for the Gailtal.

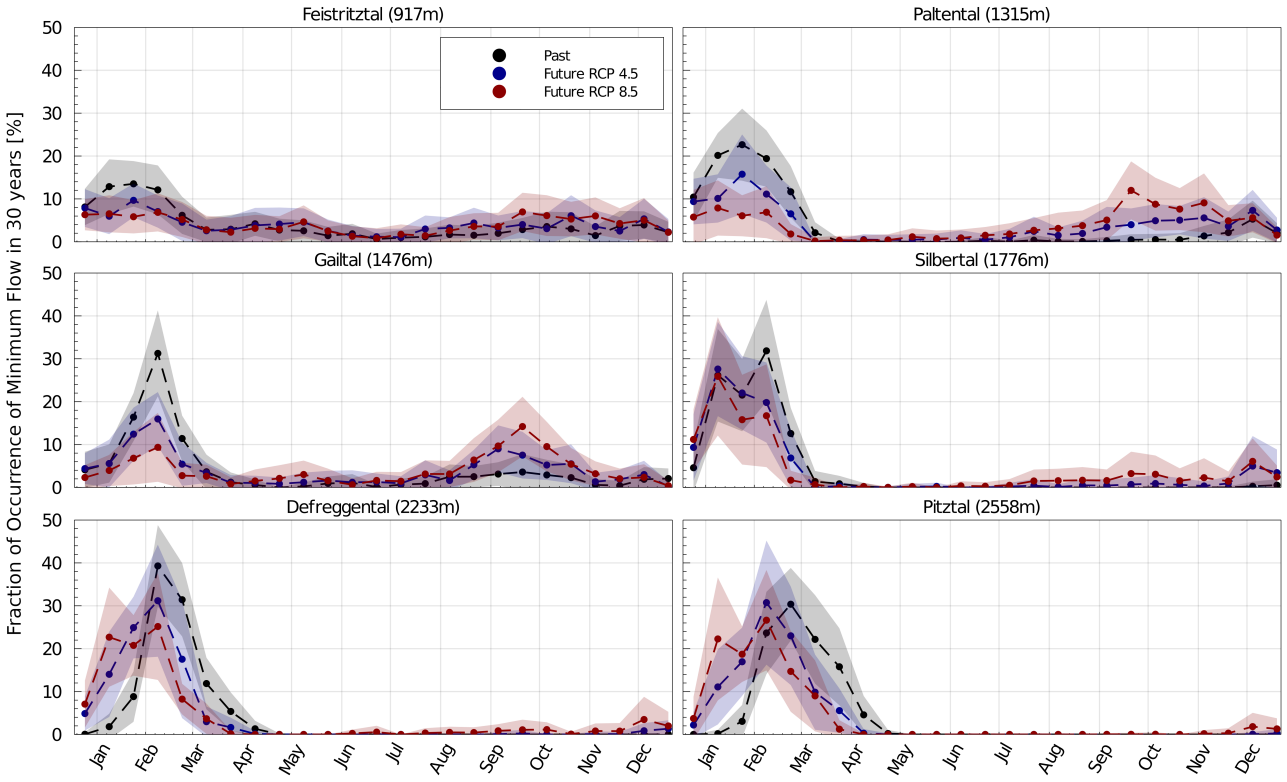

Figure 12: Simulation mean fraction of occurrences of yearly lowest 7 day flow in 30 years using time windows of 15 days, uncertainty band of 1 std is shaded, dashed lines between 15 day periods are used for better visualization.

tal from July to November for RCP 8.5. The number of days per month below the Q_{90} threshold shows a similar distribution.

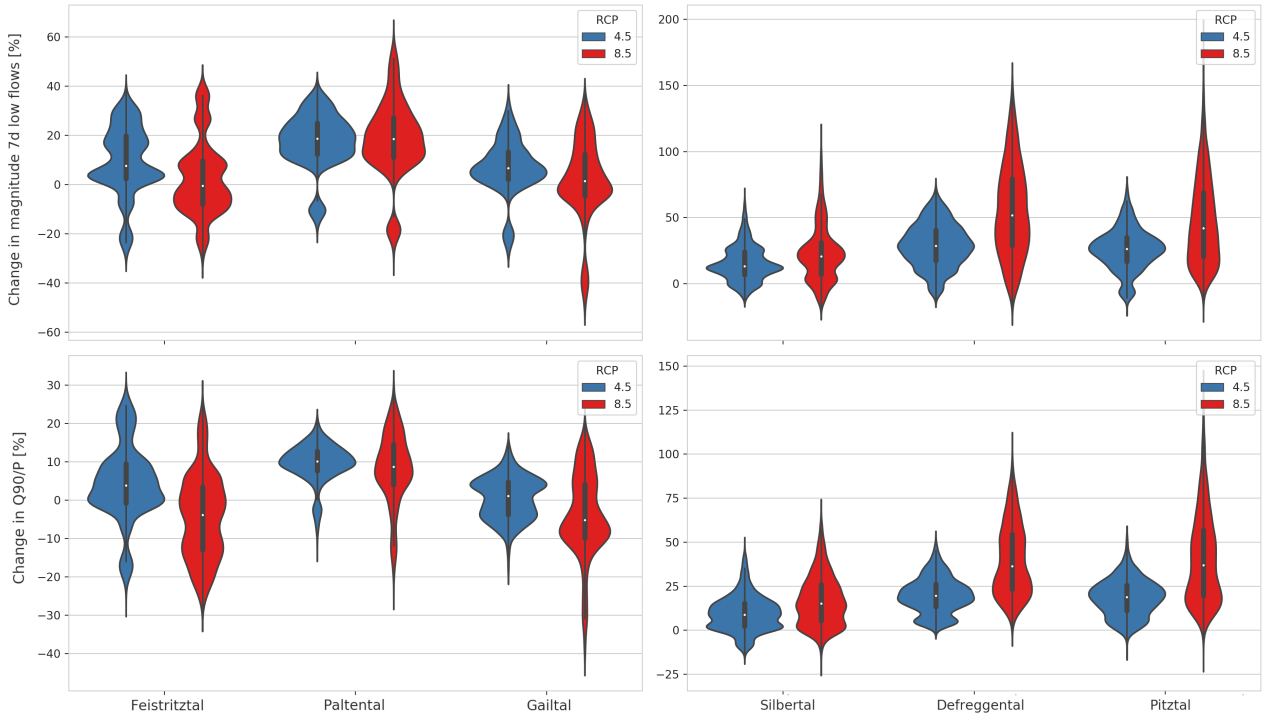

Figure 13: Relative change in magnitude of annual minimum 7 day flows (1st row) in future and relative change in ratio of Q_{90} to precipitation (2nd row) in future. Note the different scales for lower and higher elevation catchments.

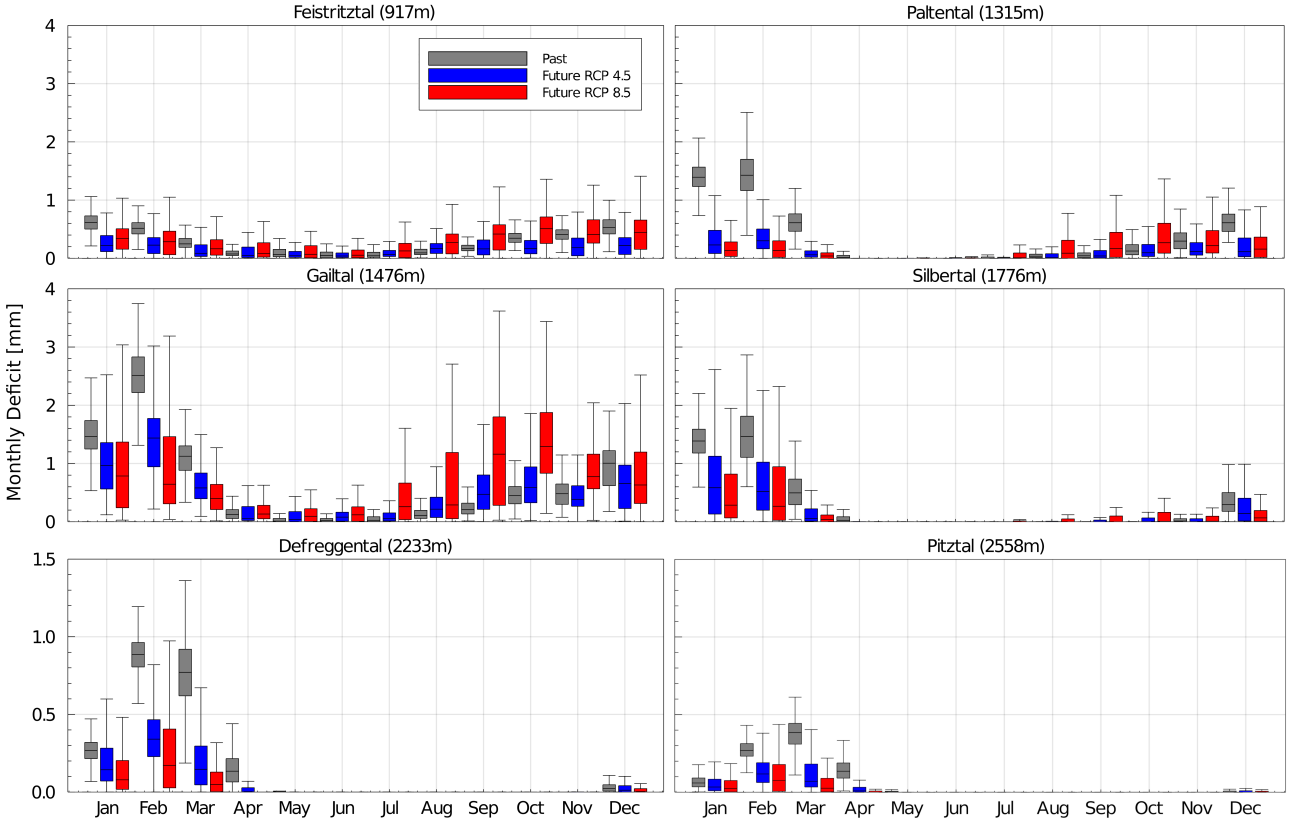

Figure 14: Monthly deficit based on Q_{90} threshold for the past and the future under RCP 4.5 and RCP 8.5: The larger the deficit, the more severe the low flows. Outliers are not shown.

3.4.5 Melt

A decrease in annual melt contribution is detected in future in all catchments ranging from 10 to 30% for

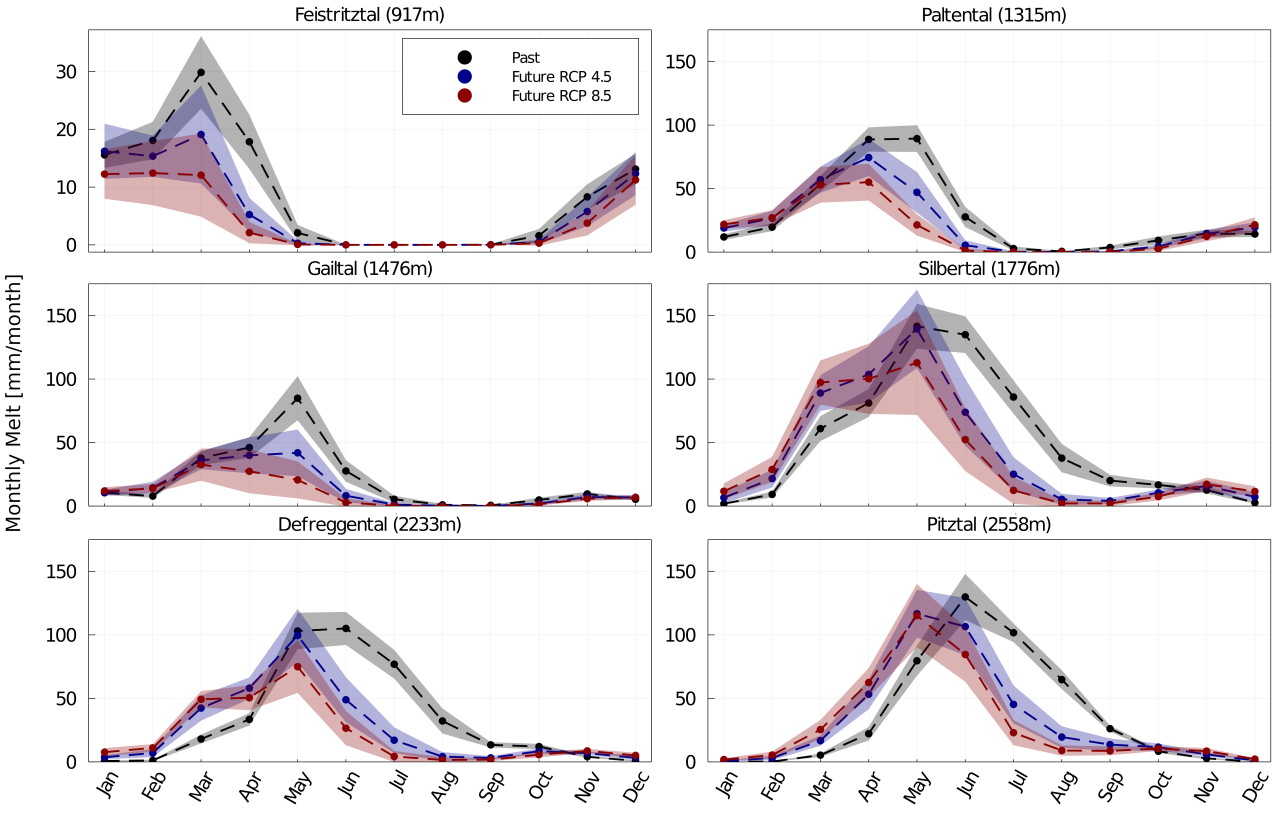

Figure 15: Monthly melt contributions in the past and future, uncertainty band of 1 std is shaded, dashed lines between the monthly values are used for better visualization.

RCP 4.5 and 20 to 55% for RCP 8.5. The results do not show the direct contribution of melt water to discharge but the contribution of melt water to the hydrological storages and processes leading to discharge. The origin of discharge was not directly followed throughout the hydrological model.

The monthly amounts of melt water for each catchment are shown in Figure 15. It can be seen that the amount of melt water in the Feistritztal is small compared to all other catchments. For the higher catchments an earlier onset of melt can be detected with a largest increase of 25mm for the Silbertal and Defreggental in March and 35mm for the Pitztal in May. Moreover, a remarkable decrease in melt in June to September is observed for the higher elevation catchments. The month with the largest melt shifts to one month earlier. Differences between the two emission scenarios are mostly visible in lower melt amounts in May to July for Silbertal and Defreggental and June to August for Pitztal, whereas melt amounts are similar for both emission scenarios in the first months of snow melt.

The same is observed for the Paltental and Gailtal, but for the Feistritztal snow melt amounts are always lower for RCP 8.5. As opposed to the higher elevation catchments no substantial increase in snow melt in the first months of the year is observed for the lower catchments.

4 Discussion

4.1 Hydroclimatic Changes

The increase in precipitation in future compared to the past contradicts climate projections for Austria used in other studies. These suggest a decrease in precipitation (Stanzel & Nachtnebel, 2010). Moreover, the modelled increase in annual discharge is not in line with results from other alpine catchments in Austria, which suggest no change or a decrease in annual discharge (Goler et al., 2016). The median increase in annual discharge of around 5% for all catchments but the Pitztal under RCP 4.5 can be explained by a precipitation increase in future of around 6%. Under RCP 8.5 the lower elevation catchments show a median change in annual discharge of -1.5 to 2% which is much lower than the precipitation increase of 4.5-7% and can be attributed to increased evaporation. In the past, the Pitztal plots above the energy limit in the Budyko framework using climate projections, but not using measured data. However, the impact on the results should be limited because a relative comparison of past and future runoff patterns is applied using climate projections for both periods.

4.2 Hydrological Changes

Regarding the partitioning of precipitation in evaporation and runoff, the decrease in mean runoff coefficient

can be attributed to increased evaporation. Changes in seasonal runoff coefficients and melt contributions are likely related (Figure 7 & 15). In seasons with decreasing melt contributions in future, spring/summer for lower/higher elevation catchments, the runoff coefficient decreases, whereas it increases in spring for higher elevation catchments, where melt contribution increase in future. This implies changes in snow contributions are more important for seasonal runoff changes than precipitation changes since precipitation increases in winter and spring. Decreases in seasonal runoff coefficient in summer and autumn can be explained by decreased runoff due to decreased precipitation. In lower elevation catchments this is evident by an increased number of minimum flow events in autumn (see Figure 12). A more in-depth discussion of relations between results of the study is given in the following sections.

4.2.1 Monthly Discharges

The results regarding changes in monthly discharges confirm previous results in the region by Laghari et al. (2012); Stanzel & Nachtnebel (2010); Tecklenburg et al. (2012), which also model an increase in winter and spring discharges and a decrease in summer discharges in alpine catchments in Austria. The largest increase in winter discharge occurs in later months for the higher catchments which supports findings by Stanzel & Nachtnebel (2010) for alpine catchments in Austria. An explanation gives the later onset of the melting season of a month or more in higher elevation catchments, visible in Figure 15, resulting in a maximum increase in discharges in later months and a later decrease in monthly discharge. Hanzer et al. (2018) simulated changes in monthly runoff in the upper part of the Pitztal and found largest increases in March by around 80% (150%) for RCP 4.5 (RCP 8.5) and largest decreases in August of around 50%, which is similar to results of this study (see Figure 8).

The increase in discharge in winter and spring months can be related to an increase in precipitation, responsible for the increase in discharge in winter (December to February), and an increase in melt contribution, mainly responsible for the discharge increase in spring (March to May). Under RCP 4.5 in high elevation catchments during spring the monthly snow melt contribution increases by around 10-35mm/month and precipitation by 1-11mm/month, leading to an increase in discharge of 10-33mm/month.

The slight increase in summer discharge (0.4-4mm/month) under RCP 4.5 in the Feistritztal marks an exception and can be explained by a large increase in precipitation in May and June (10 and 13mm/-month), which is opposed by increasing evaporation as potential evaporation increases by around 10mm/-month. As in all other catchments, under RCP 8.5 monthly discharge in summer in Feistritztal decreases (-0.5 to -4mm/month), which can be explained by a twice as large increase in potential evaporation compared to RCP 4.5, a lower increase in precipitation in May and June (7 and 2mm/month) and a decrease in precipitation in July and August (-8 and -3mm/month).

The first two months with negative change in monthly discharge are May to August under RCP 4.5 depending on the catchment. The decrease in discharge is -5 to -24mm/month and can be attributed to a decrease in melt contribution (-18 to -56mm/month) in combination with increased potential evaporation (5-12mm/month). Contrary, precipitation still increases in these months (1-24mm/month). However, for the lower elevation catchments Paltental and Gailtal in later summer (under RCP 4.5 August) the decreased precipitation (-4 and -8mm/month) in combination with increased potential evaporation (+7 and +9mm/month) is thought to be the main contributor to discharge decrease (-3 and -5mm/month) because melt contribution is negligible. The higher importance of melt contribution for summer discharge in higher elevation catchments compared to lower elevation catchments can also explain the larger decrease in summer discharge of 14-24mm/month compared to 6-13mm/month in lower elevation catchments. Moreover, a decrease in melt contribution from glaciated areas could be of great importance for the decrease in summer discharge in the Pitztal (Hanzer et al., 2018; Laurent et al., 2020). The maximum decrease in monthly discharge does not occur for the month with maximum precipitation decrease but earlier. Thus, it can be concluded that the increase in melt contribution and potential evaporation mostly influences the change in monthly runoff more than changing precipitation patterns.

The decrease in summer discharge under RCP 8.5 exceeds the decrease under RCP 4.5 by 2 to 21mm/month. This can be explained by a 0.1 to 32mm/month stronger decrease in melt contribution, an increased evaporation due to a 2-11mm/month higher potential evaporation and a mostly stronger decrease in monthly precipitation of -15 to +4mm/month under RCP 8.5. The winter and spring discharges under RCP 8.5 show an additional increase of 2 to 14mm/-month compared to RCP 4.5, explained by a 0.3 to 14mm/month larger increase in snow melt (see Figure 15), due to higher temperatures, as well as a 0.7-6mm/month larger average increase in precipitation in winter months under RCP 8.5.The Feistritztal is the only catchment with a similar model median increase in winter discharges for both emission scenarios. A possible explanation is that the larger decrease in snow contribution is balanced by the higher precipitation under RCP 8.5, resulting in a similar change in discharge under both emission scenarios.

4.2.2 Timing of High Flows

The mean timing of AMF in October for the Gailtal, and June and July for the other catchments in the past is supported by findings of Blöschl et al. (2011); Parajka et al. (2009). The high elevation catchments, show a high flood seasonality in the past due to snow melt as

flood generating process. The timing of AMF shifts significantly towards earlier occurrences in these catchments (-9 to -31 days), which is most likely induced by an earlier snow melt in future. In future the AMF occurs most often in May and beginning of June compared to mid June to early July in the past. This fits well with the shift in timing of maximum monthly melt contributions which shifts from June to May.

The autumn nival flow regime of the Gailtal is characterized by maximum flows in late spring due to snow melt and a secondary maximum of flow in autumn due to intensive precipitation (Mader et al., 1996), which translates into high flows appearing in late spring and autumn (Blöschl et al., 2011). The shift in future towards mean later occurrences in AMF in the Gailtal can be attributed on one hand to an average larger increase in precipitation in November by (+10/+16mm/month) compared to October (+2/-5mm/month) under RCP 4.5/8.5, shifting the month where most AMF occur towards later, especially for RCP 8.5. On the other hand, it can be attributed to a shift towards earlier occurrences of AMF during the start of year, seen by an increase of occurrences until mid April of 5 and 9%, under RCP 4.5 and RCP 8.5 respectively, and a decrease of occurrences by the same percentage in the months thereafter. This shift in winter and spring can be explained by an earlier snow melt in combination with increased precipitation.

The mean shift of half a month towards earlier occurrences of AMF in Feistritztal and Paltental for RCP 8.5 could be explained by multiple possible factors. Firstly, the decrease in monthly discharge from May on wards under RCP 8.5 compared to RCP 4.5 possibly leads to less maximum discharge occurring in summer. Secondly, comparing results of RCP 8.5 to RCP 4.5, the Feistritztal shows a larger increase in AMF occurrences in December to February and the Paltental in beginning November and March. This can be related to higher precipitations under RCP 8.5 in the specific months (9mm/month compared to 5mm/month in Feistritztal).

The seasonality of AMF decreases in future and the potential flood season expands, which is also suggested by Köplin et al. (2014); Schneeberger et al. (2015). This indicates that in future AMF is not only generated by snow melt or the combination of snow melt and high precipitation but more often only by precipitation. Dobler et al. (2012) found a similar increase of 3 months in potential flood season for the Lech catchment in Austria.

To conclude, the timing of AMF in high elevation catchments depends and will continue to depend mostly on snow melt. Therefore, temporal shifts in snow melt lead to substantial time shifts of AMF. This emphasizes the importance of temperature change for runoff patterns in alpine catchments. In the lower catchments, where a seasonality in timing of AMF is less pronounced today, shifts in future occur mostly due to changes in precipitation patterns, decreased flows in summer months and increased flows in winter months.

4.2.3 Magnitude of High Flows

The mean increase in magnitude of AMF for all catchments but the Paltental for RCP 4.5 is contrary to findings by Holzmann et al. (2010) who found a decrease in AMF magnitudes for catchments in Western Austria. Also, Thober et al. (2018) show a decrease in maximum discharges for the Alps under future climate conditions. However, for Swiss catchments an increase in magnitude of AMF in future was predicted by Köplin et al. (2014), whereas results of Brunner et al. (2019) indicate a decrease or no change in maximum runoff under extreme flow regimes in future in melt-dominated areas in Switzerland. A similar relative mean model increase in all catchments (around 10%) suggests increased precipitation as the underlying reason, since monthly precipitation increases for RCP 4.5 for all catchments during the main flood season (6 to 15%) and precipitation intensity rises by 5 to 18%. This is supported by findings of Schneeberger et al. (2015) for the Lech catchment in Austria where an increase in temperature without changes in precipitation only leads to minor shifts in flood intensities. A possible explanation for the low median increase in magnitude in the Paltental of 2% under RCP 4.5 with large uncertainties could be that the strong decrease in snow melt contribution in May and June of 50 and 80% opposes the increase in precipitation (9 and 7%) and maximum precipitation intensity (5%).

Interestingly, the increase in mean magnitude of AMF is lower for four out of six catchments under RCP 8.5 compared to RCP 4.5. This shows that not all changes are stronger for the higher emission scenario. A possible explanation for the lower elevation catchments, Feistritztal and Paltental, is the more than 50% larger increase of potential evaporation under RCP 8.5. This can result in a larger storage deficit which can buffer the precipitation leading to lower annual maximum flows. Moreover, the 10-30% larger decrease in snow melt contributions under RCP 8.5 counteracts the 2-6% larger increase of precipitation amounts and mostly larger changes of precipitation intensity (-1 to +15%). For the higher elevation catchments, Defreggental and Silbertal, snow contribution is important in the generation of annual maximum flows. Under RCP 8.5 the largest monthly melt contribution, which occurs in May is 113 and 75mm/month and thus is lower than for RCP 4.5 and the past, for which maximum monthly melt contributions are 140 and 100mm/month (see Figure 15). This decrease in melt contribution, and possibly higher potential evaporation, seem to be more important for change in AMF magnitudes under RCP 8.5 than the increase in precipitation intensities of 14-20% for RCP 8.5 compared to 5-16% for RCP 4.5. A reason for the similar increase in AMF magnitude for the Pitztal across RCP 4.5 and 8.5 could be that the maximum monthly melt contribution remains similar for both emission scenarios (115mm/month) due

to the high altitude of the catchment. In conclusion, the changes induced by increased temperature seem to have a larger effect on change in AMF magnitudes under RCP 8.5 than changes in precipitation, which seem to be more important for AMF magnitude increases under RCP 4.5.

The increase in magnitude of AMF is larger for high return periods, especially under RCP 8.5. However, also the uncertainty is higher. The increase in discharge for a 30 year return period modelled in this study is much larger than the increase in HQ100 of 4% for the Gailtal for the mid of the 21st century suggested by Blöschl et al. (2011). For catchments in the region of Silbertal, Defreggental and Pitztal the study by Blöschl et al. (2011) suggests a decrease in HQ100 which opposes results of this study. A strongly above-average increase in magnitudes of very rare discharge events could be explained by a relatively stronger increase in magnitudes of maximum extreme monthly precipitation intensities occurring once in 30 years (up to +55%) compared to a lower increase by +5 to +22% of mean maximum precipitation intensities over 30 years.

However, a large uncertainty surrounds discharge magnitude of high return periods as can be seen by the uncertainty bands in Figure 11. One reason for the uncertainties is that the evaluation of extreme events depends highly on the chosen time period. Other studies conclude that the natural variability in magnitude of high flows exceeds the change due to climate change which increases uncertainty especially for high return periods (Dobler et al., 2012; Blöschl et al., 2011).

4.2.4 Low Flows

In the higher alpine catchments a shift towards earlier occurrences of low flows to January and February can be explained by an increase in melt contributions in February to April which translates into an increase in monthly discharge. The minimum flows occur before melting starts. In the lower catchments the shift in timing of minimum flows from winter to autumn can be related to an increased potential evaporation with a largest increase of 7-13mm/month (RCP 4.5) or 12-24mm/month (RCP 8.5) in July as well as mostly decreasing monthly precipitation in July to September of -8 to +8mm/month (RCP 4.5) and -12 to 0mm/month (RCP 8.5). Thus, an increased storage deficit in the unsaturated zone in late summer due to increased evaporation possibly leads to longer storage of precipitation before release as discharge. This is also reflected by the increasing monthly deficit (0 to +1mm/month) in autumn months as shown in Figure 14. The reduction of monthly deficit in winter and an increase in monthly deficit in late summer is in line with findings by Goler et al. (2016) for other Austrian catchments, which predict a reduction of days below the Q_{95} threshold in winter but an increase in summer.

The magnitude of minimum yearly discharges mostly increases in future. Similar results are found when evaluating the change of Q_{90} relative to precipitation which agrees with findings of previous studies in the Alps (Brunner et al., 2019; Laaha et al., 2016; Marx et al., 2018; Parajka et al., 2016). An explanation for the mean decrease of 6% in ratio of Q_{90} to precipitation in the Feistritztal and Gailtal for RCP 8.5 is that annual precipitation increases by 6 and 4%, whereas the value of Q_{90} does not change considerably on average, which can be related to an increase in temperature and decrease in precipitation in the summer months. Therefore, magnitudes of Q_{90} in these catchments depend on low flows in summer rather than low flows in winter in the far future. The increase in magnitude of minimum yearly flows in the other catchments by 12-50% (0.07-0.7mm/d) can be related to an increase in lowest monthly discharges by around 30 to 110% due to higher precipitation amounts and decreased amount of water stored as snow as explained earlier. This also explains a decreased water deficit in winter months in future of 0.05 to 0.93mm/month on average.

4.3 Societal Impacts

Changes in monthly discharges impact seasonal water availability. In future there will be more water available in winter and less in summer. This could lead to a mismatch between water supply and water demand as mountain regions of the Alps are classified as supportive for the lowlands (Viviroli et al., 2007). However, the Alps are identified as basins where present water demands can also be met in 2060 (Mankin et al., 2017). Therefore, water scarcity due to changes in runoff dynamics in the Alps seems unlikely. Changes in discharge also impact hydro-power production. This study found mostly an increase in annual runoffs in future which may have a positive impact on hydropower generation. Nevertheless, seasonal changes can lead to decreased energy production in summer and autumn and increased energy production in winter and spring. Management schemes of hydro-power production might have to be adapted to changing water availability. Adaptation measures are likely to be higher for RCP 8.5. Regarding annual maximum flows, an increase of magnitudes of maximum flows might require changes in flood risk assessments and could potentially impact structures designed for lower flood estimates. Moreover, an extension of the potential flood season could lead to less predictability of flood events in future.

4.4 Climate Projection Uncertainty

The results of individual climate projections were compared to investigate whether a specific climate projection (see Table 2) corresponds to extreme changes across catchments. Regarding changes in mean annual temperature, Projection-1 shows the lowest and Projection-12 the largest increase in temperature under RCP 8.5. Under RCP 4.5 Projection-13 presents the lowest increase in temperature, whereas projections with

the largest increase in temperature differ per catchment. Projection-10 displays the largest decrease in annual precipitation under both emission scenarios for all catchments of around 10% (see Figure 4), while no single projection displays the largest increase in precipitation across catchments. To distinguish relationships between modelled hydrological characteristics and projections, monthly, maximum and minimum runoff per climate projection were compared using a cumulative distribution function.

Generally, no single climate projection was found to lead to largest or lowest changes across catchments or across emission scenarios. For extreme changes of monthly discharge in summer and early autumn, extreme changes in precipitation seem to be crucial because the projection with largest decrease/increase in precipitation yielded largest/lowest decreases in monthly discharges. For changes in other months, no relationship between the most extreme changes and a certain projection was found. Looking at the magnitude of annual minimum and maximum flows, the projection with strongest decrease in precipitation (Projection-10) produces the lowest changes, whereas the projection with largest increase in precipitation mostly results in the largest increases in magnitudes. Regarding timing of AMF, the lowest/largest shift towards earlier occurrences is present using the projections with the largest increase in precipitation/temperature under RCP 8.5. The relationship of projections and timing of minimum flows is less clear.

In conclusion, there are substantial differences in modelled changes between climate projections, e.g. changes in mean timing of AMF vary between -40 to +5 days for Pitztal and -60 to -5 days for the Silbertal depending on the projection utilized. The median relative change in magnitude of AMF varies from 4-40% for the Pitztal and between 6-34% for the Gailtal. Thus, the employment of an ensemble of climate projections is indispensable. Extremes in changes for different catchments and emission scenarios often cannot be traced back to a single projection. However, Projection-10 is the single projection resulting in most extreme changes across catchments due a substantial decrease in precipitation.

4.5 Uncertainty & Limitations

There are several uncertainties and limitations involved in this study, mainly regarding input data and model choices. Input data from in situ point measurements likely contain measurement errors. Firstly, precipitation data was derived from only one to four precipitation gauges per catchment. Therefore, total precipitation amounts in the catchment could be wrong, especially during convective storms or when altitudes of precipitation gauges do not represent the altitude range of the catchment. This could be one explanation for the mismatch of precipitation and discharge data in the Silbertal and Defreggental. Moreover, this uncertainty in data possibly also causes an underestimation of peak discharges which was detected during calibration. Therefore, results regarding magnitude of maximum discharges are probably less reliable and are likely the lower limits of change. Secondly, an unknown amount of water is diverted from the Pitztal, which resulted in increased uncertainty during calibration of this catchment.

During the implementation of the model many choices had to be made regarding the representation of processes and specific equations (see Appendix X). Each decision was taken carefully but still encompasses uncertainties. For example, the choice of calculation method for the potential evaporation influences the results and thus introduces uncertainty (Seiller & Anctil, 2016). Melt was represented by a degree-day method which is a major simplification of reality. Sublimation was not considered in the model although it can have a significant effect in high elevation areas (MacDonald et al., 2010). Also snow redistribution by gravity or wind was not considered. These could be explanations for the snow accumulation over years during modelling of the past at the highest elevations in the Pitztal and to a lesser extent in the Defreggental and Silbertal. Nevertheless, snow accumulation to some extend is realistic in Pitztal and Defreggental due to the presence of glaciers. Another uncertainty arises from calibrating the model with measured data but using projection data for the future. To reduce this limitation data from the same location was used. Nevertheless, temperature of climate projections underestimated the measured temperatures in the past for high elevation catchments. This could be a possible explanation for the induced error in the position of the Pitztal in the Budyko framework (see Figure 5) because lower temperatures lead to enhanced snow accumulation and decreased runoff.

Another uncertainty for future changes in runoff patterns besides climate change is land use change. Natural and human induced land use change can alter hydrological responses significantly (Jaramillo, 2015; Thieken et al., 2016). Land use is incorporated in the model by different HRUs for bare, forested and grassland hillslopes which differ in parameters for landscape dependent processes (see Figure 2). Land use change could be represented by changing the areal extents of specific HRUs. Nonetheless, land use change was not considered in this study, except for glacier retreat, due to time constraints and large uncertainties related to land use change in future.

One of the largest uncertainties in climate impact assessment – the utilized climate projection – has been taken into account in this study compared to previous studies in the region by using an ensemble of climate projections. It should be stressed that all results of this study depend on the climate projections used.

5 Conclusion

The aim of this study was to investigate the effect of climate change on runoff patterns in alpine catchments in Austria at the end of this century focusing on catchments at different altitudes. The results provide evidence of significant changes in runoff patterns in alpine catchments due to climate change in future. Future changes are more pronounced for high elevation catchments because they highly depend on snow dynamics.

For high elevation catchments, a substantial shift in timing of annual maximum flows to earlier occurrences up to a month and an extension of the potential flood season by one to three months was found. For lower elevation catchments, shifts in timing are less clear. The Gailtal is the only catchment exhibiting a significant shift of around one month to later occurrences of AMF due to substantial shifts in precipitation. A mean increase in AMF magnitudes was determined with mostly larger changes for RCP 4.5 compared to RCP 8.5. The Gailtal and Pitztal exhibit the largest increase in maximum AMF magnitudes in the time period by 40% and 32% respectively, although uncertainty is high.

Another main finding of this study is a shift to towards earlier minimum yearly flows in January and February in high elevation catchments, whereas in lower elevation catchments minimum yearly flows shift from the beginning of the year to autumn. While all catchments show an increase in magnitudes of minimum flows under RCP 4.5, no change or decreases are found for two of the lower elevation catchments under RCP 8.5.

Future research could focus on modelling climate change under different land use change scenarios in alpine catchments to explore the importance of land use change and identify scenarios under which climate change impacts are intensified or weakened. Moreover, it would be worthwhile to explicitly investigate the effect of future hydrological changes in high elevation catchments on society and inhabitants.

Glossary

AMF Annual maximum flow.

GCM General circulation model.

HRU Hydrological response unit.

NSE Nash Sutcliffe efficiency.

RCM Regional climate model.

RCP Representative concentration pathway.

References

Abermann, J., Fischer, A., Lambrecht, A., & Geist, T. (2010). On the potential of very high-resolution repeat DEMs in glacial and periglacial environments. *The Cryosphere*, *4*(1), 53.

Abudu, S., Sheng, Z.-p., Cui, C.-l., Saydi, M., Sabzi, H.-Z., & King, J. P. (2016). Integration of aspect and slope in snowmelt runoff modeling in a mountain watershed. *Water Science and Engineering*, *9*(4), 265–273.

Addor, N., Rössler, O., Köplin, N., Huss, M., Weingartner, R., & Seibert, J. (2014). Robust changes and sources of uncertainty in the projected hydrological regimes of Swiss catchments. *Water Resources Research*, *50*(10), 7541–7562.

Aich, V., Liersch, S., Vetter, T., Huang, S., Tecklenburg, J., Hoffmann, P., … others (2014). Comparing impacts of climate change on streamflow in four large African river basins. *Hydrology and Earth System Sciences*, *18*(4).

Barnett, T. P., Adam, J. C., & Lettenmaier, D. P. (2005). Potential impacts of a warming climate on water availability in snow-dominated regions. *Nature*, *438*(7066), 303–309.

Bavay, M., Grünewald, T., & Lehning, M. (2013). Response of snow cover and runoff to climate change in high Alpine catchments of Eastern Switzerland. *Advances in Water Resources*, *55*, 4–16.

Beven, K., & Binley, A. (1992). The future of distributed models: model calibration and uncertainty prediction. *Hydrological Processes*, *6*(3), 279–298.

Beven, K., & Westerberg, I. (2011). On red herrings and real herrings: disinformation and information in hydrological inference. *Hydrological Processes*, *25*(10), 1676–1680.

Blahušiaková, A., Matoušková, M., Jenicek, M., Ledvinka, O., Kliment, Z., Podolinská, J., & Snopková, Z. (2020). Snow and climate trends and their impact on seasonal runoff and hydrological drought types in selected mountain catchments in Central Europe. *Hydrological Sciences Journal*, *65*(12), 2083–2096.

Blöschl, G., Hall, J., Parajka, J., Perdigão, R. A., Merz, B., Arheimer, B., … others (2017). Changing climate shifts timing of European floods. *Science*, *357*(6351), 588–590.

Blöschl, G., Hall, J., Viglione, A., Perdigão, R. A., Parajka, J., Merz, B., … others (2019). Changing climate both increases and decreases European river floods. *Nature*, *573*(7772), 108–111.

Blöschl, G., Viglione, A., Merz, R., Parajka, J., Salinas, J., & Schöner, W. (2011). Auswirkungen des Klimawandels auf Hochwasser und Niederwasser. *Österreichische Wasser-und Abfallwirtschaft*, *63*(1-2), 21–30.

Braithwaite, R. J. (2008). Temperature and precipitation climate at the equilibrium-line altitude of glaciers expressed by the degree-day factor for melting snow. *Journal of Glaciology*, *54*(186), 437–444.

Brunetti, M., Lentini, G., Maugeri, M., Nanni, T., Auer, I., Boehm, R., & Schoener, W. (2009). Climate variability and change in the Greater Alpine Region over the last two centuries based on multivariable analysis. *International Journal of Climatology: A Journal of the Royal Meteorological Society*, *29*(15), 2197–2225.

Brunner, M. I., Farinotti, D., Zekollari, H., Huss, M., & Zappa, M. (2019). Future shifts in extreme flow regimes in Alpine regions. *Hydrology and Earth System Sciences*, *23*(11), 4471–4489.

Cauvy-Fraunié, S., & Dangles, O. (2019). A global synthesis of biodiversity responses to glacier retreat. *Nature Ecology & Evolution*, *3*(12), 1675–1685.

Criss, R. E., & Winston, W. E. (2008). Do Nash values have value? Discussion and alternate proposals. *Hydrological Processes*, *22*(14), 2723–2725.

Dobler, C., Bürger, G., & Stötter, J. (2012). Assessment of climate change impacts on flood hazard potential in the Alpine Lech watershed. *Journal of Hydrology*, *460*, 29–39.

Efstratiadis, A., & Koutsoyiannis, D. (2010). One decade of multiobjective calibration approaches in hydrological modelling: a review. *Hydrological Sciences Journal*, *55*(1), 58–78.

Euser, T., Winsemius, H., Hrachowitz, M., Fenicia, F., Uhlenbrook, S., & Savenije, H. (2013). A framework to assess the realism of model structures using hydrological signatures. *Hydrology and Earth System Sciences*, *17*(5).

Finger, D., Vis, M., Huss, M., & Seibert, J. (2015). The value of multiple data set calibration versus model complexity for improving the performance of hydrological models in mountain catchments. *Water Resources Research*, *51*(4), 1939–1958.

Gao, H., Ding, Y., Zhao, Q., Hrachowitz, M., & Savenije, H. H. (2017). The importance of aspect for modelling the hydrological response in a glacier catchment in Central Asia. *Hydrological Processes*, *31*(16), 2842–2859.

Gao, H., Hrachowitz, M., Fenicia, F., Gharari, S., & Savenije, H. (2014). Testing the realism of a topography-driven model (FLEX-Topo) in the nested catchments of the Upper Heihe, China. *Hydrology and Earth System Sciences*, *18*(5), 1895.

Gharari, S., Hrachowitz, M., Fenicia, F., Gao, H., & Savenije, H. (2014). Using expert knowledge to increase realism in environmental system models can dramatically reduce the need for calibration. *Hydrology and Earth System Sciences*, *18*(12).

Girons Lopez, M., Vis, M. J., Jenicek, M., Griessinger, N., & Seibert, J. (2020). Assessing the degree of detail of temperature-based snow routines for runoff modelling in mountainous areas in central Europe. *Hydrology and Earth System Sciences*, *24*(9), 4441–4461.

Goler, R. A., Frey, S., Formayer, H., & Holzmann, H. (2016). Influence of climate change on river discharge in Austria. *Meteorologische Zeitschrift*, *25*(5), 621–626.

Griessinger, N., Seibert, J., Magnusson, J., & Jonas, T. (2016). Assessing the benefit of snow data assimilation for runoff modeling in Alpine catchments. *Hydrology and Earth System Sciences*, *20*(9), 3895–3905.

Hall, D. K., & Riggs, G. A. (2016). MODIS/Terra Snow Cover Daily L3 Global 500m SIN Grid, Version 6. *NASA National Snow and Ice Data Center Distributed Active Archive Center.*. Retrieved 2020-05-16, from https://doi.org/10.5067/MODIS/MOD10A1.006

Hanzer, F., Förster, K., Nemec, J., & Strasser, U. (2018). Projected cryospheric and hydrological impacts of 21st century climate change in the Ötztal Alps (Austria) simulated using a physically based approach. *Hydrology and Earth System Sciences*, *22*(2), 1593–1614.

He, Z., Parajka, J., Tian, F., & Blöschl, G. (2014). Estimating degree day factors from MODIS for snowmelt runoff modeling. *Hydrology and Earth System Sciences*, *11*(7).

Her, Y., Yoo, S.-H., Cho, J., Hwang, S., Jeong, J., & Seong, C. (2019). Uncertainty in hydrological analysis of climate change: multi-parameter vs. multi-GCM ensemble predictions. *Scientific Reports*, *9*(1), 1–22.

Holzmann, H., Lehmann, T., Formayer, H., & Haas, P. (2010). Auswirkungen möglicher Klimaänderungen auf Hochwasser und Wasserhaushaltskomponenten ausgewählter Einzugsgebiete in Österreich. *Österreichische Wasser-und Abfallwirtschaft*, *62*(1-2), 7–14.

Hrachowitz, M., Fovet, O., Ruiz, L., Euser, T., Gharari, S., Nijzink, R., ... Gascuel-Odoux, C. (2014). Process consistency in models: The importance of system signatures, expert knowledge, and process complexity. *Water Resources Research*, *50*(9), 7445–7469.

IPCC. (2019). *IPCC Special Report on the Ocean and Cryosphere in a Changing Climate (IPCC, 2019)* (Tech. Rep.).

Jaramillo, F. (2015). *Changes in the Freshwater System: Distinguishing Climate and Landscape Drivers* (Unpublished doctoral dissertation). Department of Physical Geography, Stockholm University.

Jenicek, M., Seibert, J., & Staudinger, M. (2018). Modeling of future changes in seasonal snowpack and impacts on summer low flows in alpine catchments. *Water Resources Research*, *54*(1), 538–556.

Köplin, N., Schädler, B., Viviroli, D., & Weingartner, R. (2014). Seasonality and magnitude of floods in Switzerland under future climate change. *Hydrological Processes*, *28*(4), 2567–2578.

Kormann, C., Francke, T., & Bronstert, A. (2015). Detection of regional climate change effects on alpine hydrology by daily resolution trend analysis in Tyrol, Austria. *Journal of Water and Climate Change*, *6*(1), 124–143.

Laaha, G., Parajka, J., Viglione, A., Koffler, D., Haslinger, K., Schöner, W., ... Blöschl, G. (2016). A three-pillar approach to assessing climate impacts on low flows. *Hydrology and Earth System Sciences*, *20*(9), 3967.

Laghari, A., Vanham, D., & Rauch, W. (2012). To what extent does climate change result in a shift in Alpine hydrology? A case study in the Austrian Alps. *Hydrological Sciences Journal*, *57*(1), 103–117.

Lambrecht, A., & Kuhn, M. (2007). Glacier changes in the Austrian Alps during the last three decades, derived from the new Austrian glacier inventory. *Annals of Glaciology*, *46*, 177–184.

Laurent, L., Buoncristiani, J.-F., Pohl, B., Zekollari, H., Farinotti, D., Huss, M., ... Pergaud, J. (2020). The impact of climate change and glacier mass loss on the hydrology in the Mont-Blanc massif. *Scientific Reports*, *10*(1), 1–11.

Leng, G., Tang, Q., & Rayburg, S. (2015). Climate change impacts on meteorological, agricultural and hydrological droughts in China. *Global and Planetary Change*, *126*, 23–34.

MacDonald, M., Pomeroy, J., & Pietroniro, A. (2010). On the importance of sublimation to an alpine snow mass balance in the Canadian Rocky Mountains. *Hydrology and Earth System Sciences*, *14*(7), 1401.

Mader, H., Steidl, T., & Wimmer, R. (1996). Abflußregime österreichischer Fließgewässer. *Wien, AUT: Umweltbundesamt*.

Mankin, J. S., Viviroli, D., Mekonnen, M. M., Hoekstra, A. Y., Horton, R. M., Smerdon, J. E., & Diffenbaugh, N. S. (2017). Influence of internal variability on population exposure to hydroclimatic changes. *Environmental Research Letters*, *12*(4), 044007.

Marty, C., Schlogl, S., Bavay, M., & Lehning, M. (2017). How much can we save? Impact of different emission scenarios on future snow cover in the Alps. *The Cryosphere*, *11*, 517–529.

Marx, A., Kumar, R., Thober, S., Rakovec, O., Wanders, N., Zink, M., ... Samaniego, L. (2018). Climate change alters low flows in Europe under global warming of 1.5, 2, and 3 C. *Hydrology and Earth System Sciences*, *22*(2), 1017–1032.

Mostbauer, K., Kaitna, R., Prenner, D., & Hrachowitz, M. (2018). The temporally varying roles of rainfall, snowmelt and soil moisture for debris flow initiation in a snow-dominated system. *Hydrology and Earth System Sciences*, *22*(6), 3493–3513.

Nash, J. E., & Sutcliffe, J. V. (1970). River flow forecasting through conceptual models part I—A discussion of principles. *Journal of Hydrology*, *10*(3), 282–290.

Oudin, L., Hervieu, F., Michel, C., Perrin, C., Andréassian, V., Anctil, F., & Loumagne, C. (2005). Which potential evapotranspiration input for a lumped rainfall–runoff model?: Part 2—Towards a simple and efficient potential evapotranspiration model for rainfall–runoff modelling. *Journal of Hydrology*, *303*(1-4), 290–306.

Parajka, J., Blaschke, A. P., Blöschl, G., Haslinger, K., Hepp, G., Laaha, G., ... Zessner, M. (2016). Uncertainty contributions to low-flow projections in Austria. *Hydrology and Earth System Sciences*, *20*(5), 2085.

Parajka, J., Kohnová, S., Merz, R., Szolgay, J., Hlavčová, K., & Blöschl, G. (2009). Comparative analysis of the seasonality of hydrological characteristics in Slovakia and Austria/Analyse comparative de la saisonnalité de caractéristiques hydrologiques en Slovaquie et en Autriche. *Hydrological Sciences Journal*, *54*(3), 456–473.

Prenner, D., Hrachowitz, M., & Kaitna, R. (2019). Trigger characteristics of torrential flows from high to low alpine regions in Austria. *Science of The Total Environment*, *658*, 958–972.

Prenner, D., Kaitna, R., Mostbauer, K., & Hrachowitz, M. (2018). The value of using multiple hydrometeorological variables to predict temporal debris flow susceptibility in an alpine environment. *Water Resources Research*, *54*(9), 6822–6843.

Rango, A., & Martinec, J. (1995). Revisiting the degree-day method for snowmelt computations. *Water Resources Bulletin*, *31*(4), 657–669.

Savenije, H. H. (2010). HESS Opinions "Topography driven conceptual modelling (FLEX-Topo)". *Hydrology and Earth System Sciences*, *14*(12), 2681.

Schaefli, B., Manso, P., Fischer, M., Huss, M., & Farinotti, D. (2019). The role of glacier retreat for Swiss hydropower production. *Renewable Energy*, *132*, 615–627.

Schneeberger, K., Dobler, C., Huttenlau, M., & Stötter, J. (2015). Assessing potential climate change impacts on the seasonality of runoff in an Alpine watershed. *Journal of Water and Climate Change*, *6*(2), 263–277.

Seibert, J., & Vis, M. J. (2012). Teaching hydrological modeling with a user-friendly catchment-runoff-model software package. *Hydrology and Earth System Sciences*, *16*(9), 3315–3325.

Seiller, G., & Anctil, F. (2016). How do potential evapotranspiration formulas influence hydrological projections? *Hydrological Sciences Journal*, *61*(12), 2249–2266.

Stanzel, P., & Nachtnebel, H. (2010). Mögliche Auswirkungen des Klimawandels auf den Wasserhaushalt und die Wasserkraftnutzung in Österreich. *Österreichische Wasser-und Abfallwirtschaft*, *62*(9-10), 180–187.

Switanek, M. B., Troch, P. A., Castro, C. L., Leuprecht, A., Chang, H.-I., Mukherjee, R., & Demaria, E. M. (2017). Scaled distribution mapping: a bias correction method that preserves raw climate model projected changes. *Hydrology and Earth System Sciences*, *21*(6), 2649–2649.

Tecklenburg, C., Francke, T., Kormann, C., & Bronstert, A. (2012). Modeling of water balance response to an extreme future scenario in the Ötztal catchment, Austria. *Advances in Geosciences*, *32*, 63–68.

Thieken, A. H., Cammerer, H., Dobler, C., Lammel, J., & Schöberl, F. (2016). Estimating changes in flood risks and benefits of non-structural adaptation strategies-a case study from Tyrol, Austria. *Mitigation and Adaptation Strategies for Global Change*, *21*(3), 343–376.

Thober, S., Kumar, R., Wanders, N., Marx, A., Pan, M., Rakovec, O., ... Zink, M. (2018). Multi-model ensemble projections of European river floods and high flows at 1.5, 2, and 3 degrees global warming. *Environmental Research Letters*, *13*(1), 014003.

Thornthwaite, C. W. (1948). An approach toward a rational classification of climate. *Geographical Review*, *38*(1), 55–94.

Viviroli, D., Dürr, H. H., Messerli, B., Meybeck, M., & Weingartner, R. (2007). Mountains of the world, water towers for humanity: Typology, mapping, and global significance. *Water Resources Research*, *43*(7).

Vormoor, K., Rössler, O., Bürger, G., Bronstert, A., & Weingartner, R. (2017). When timing matters-considering changing temporal structures in runoff response surfaces. *Climatic Change*, *142*(1-2), 213–226.

Young, A., Round, C., & Gustard, A. (2000). Spatial and temporal variations in the occurrence of low flow events in the UK. *Hydrology and Earth System Sciences*, *4*(1), 35-45.

Zekollari, H., Huss, M., & Farinotti, D. (2019). Modelling the future evolution of glaciers in the European Alps under the EURO-CORDEX RCM ensemble. *The Cryosphere*, *13*(4), 1125–1146.

6 Appendices

A Description of Hydrological Model

In the following the hydrological model structure and the underlying assumptions will be described and the corresponding equations provided.

The temperature lapse rate is set to 0.006 °C/m (e.g. Gao et al. (2014)) to account for decreasing temperature with increasing elevation (see Eq. 1 where H_T defines the height at which temperature was measured (T_{meas}) and T_e the tempeartue at elevation H_e). A constant temperature lapse rate is assumed although in reality the lapse rate changes with season. However, a representation as a sine function of this seasonality does not improve model performance (Girons Lopez et al., 2020).

$$T_e = T_{meas} - 0.006 \cdot (H_e - H_T) \tag{1}$$

A threshold temperature (T_{thresh}) is employed to split precipitation into rain and snow. In the following two paragraphs the representation of interception and snow in the model is described. These two processes are run per elevation zone and the combined output of the elevation zones is used as input for the other processes in the model (see Figure main paper).

A.1 Interception

The water stored in the interception reservoir (S_{int}) increases if precipitation is present as rain (P_{rain}) and decreases by interception evaporation (E_{int}) and outflow of water (P_{eff}) (Eq. 2).

The interception of precipitation by vegetation is represented as a threshold process because leaves can only hold a certain amount of water. If the interception capacity (I_{max}) is exceeded, excess water leaves the storage (P_{eff}) (Eq. 3) . Afterwards water in the interception reservoir can evaporate (Eq. 4). The amount is limited by the water stored in the reservoir. Moreover, a limit of 50% of the potential evaporation is set to make the model more realistic. Thus, on cool humid days not all water potentially able to evaporate, evaporates from the interception storage but also soil evaporation can occur. Interception only takes place if temperature is above the threshold temperature which means precipitation enters the system as rain. For the bare rock HRU the process of interception is neglected as it is assumed to be negligible due to sparse vegetation.

$$\frac{dS_{int}}{dt} = P_{rain} - E_{int} - P_{eff} \tag{2}$$

$$P_{eff} = max(S_{int} - I_{max}, 0) \tag{3}$$

$$E_{int} = min(0.5 \cdot E_{pot}, S_{int}) \tag{4}$$

A.2 Snow

The changes in the snow storage (S_{snow}) are represented by the input of snow (P_{snow}) if the temperature is below the threshold temperature and the output of melt water (M_{snow}) if temperature is above the threshold temperature (Eq. 5). The bare rock HRU also has a glacier storage ($S_{glacier}$, Eq. 6).

$$\frac{dS_{snow}}{dt} = P_{snow} - M_{snow} \tag{5}$$

$$\frac{dS_{glacier}}{dt} = P_{snow} - M_{glacier} \tag{6}$$

The melt process which happens at temperatures above the threshold temperature is simulated with a degree-day approach. In this study it is assumed that the degree-day factor (DDF) (F_{melt}) is constant in time and space. Studies have shown that DDF increases during melt season, differs in different vegetation (Rango & Martinec, 1995), is correlated with elevation (He et al., 2014) and aspects of slopes. However, Griessinger et al. (2016) obtained similar results for a fixed DDF and a time-varying DDF for catchments with mean elevation below 2000m, Finger et al. (2015) showed that model performance does not increase with increasing complexity (including aspect or difference in vegetation) and Gao et al. (2017) show that including aspects does not improve the model performance but increases its spatial transferability. On the other hand, Abudu et al. (2016) illustrates that including aspects and slope slightly increased model performance. Girons Lopez et al. (2020) found a slight increase of model performance for a seasonal DDF. Yet, when evaluating increased model complexity against increased performance it was decided to implement a fixed DDF in order to keep the model simple.The melt process is represented by an exponential function as suggested by Girons Lopez et al. (2020) where M_M is the

parameter to control for the smoothness of the snowmelt transition (Eq. 7) to increase the model performance. The process is limited by the amount of water stored in the snow reservoir (Eq. 8) whereas the process is unlimited for glaciers (Eq. 9). The threshold for melt was the same as the threshold for partitioning between rainfall and snow.

$$M = F_{melt} \cdot M_M(\frac{T - T_{thresh}}{M_M} + ln(1 + \exp(-\frac{T - T_{thresh}}{M_M})) \tag{7}$$

$$M_{snow} = min(M, S_{snow}) \tag{8}$$

$$M_{glacier} = M \tag{9}$$

In the bare rock HRU, glaciers can exist, which are described as an unlimited reservoir. Glacial melting depends on the same DDF as snow melting (Eq. 9). Studies suggest a higher melt factor for glaciers than for snow (Braithwaite, 2008; He et al., 2014; Gao et al., 2017), because ice has a lower albedo than fresh snow which results in increased melting. However, glaciers are snow covered during a long period of the year. Thus, I decided to use the same melt factor in order to not further increase the number of parameters. The total melt is the combination of snow and glacier melt according to the areal extend (Eq. 10.

$$M_{tot} = M_{snow} \cdot (1 - area_{gl}) + M_{glacier} \cdot area_{gl} \tag{10}$$

The melt water is combined with the outflow of the interception reservoir over all elevation zones according to their areal extents.

$$P_{eff,tot} = \sum_{i=1}^{Elevations} P_{eff} + \sum_{i=1}^{Elevations} M_{tot} \tag{11}$$

A.3 Unsaturated Zone

The change in soil storage (S_{soil}) is defined by the water entering the unsaturated zone (q_{soil}) and the evaporation/transpiration of the soil (E_{soil}).

$$\frac{dS_{soil}}{dt} = q_{soil} - E_{soil} \tag{12}$$

The amount of water entering the soil (q_{soil}) is dependent on the water already stored in the reservoir and the maximum capacity of the soil storage (Eq. 13). The more water there is already stored in the reservoir, the less water will be stored. The relation is described by a monotonous increasing function for C_r (Eq. 14).

$$q_{soil} = min((1 - C_r) \cdot P_{eff,tot}, S_{soil,max} - S_{soil}) \tag{13}$$

$$C_r = 1 - (1 - \frac{S_{soil}}{S_{soil,max}})^{\beta} \tag{14}$$

The excess water is either diverted to the fast reservoir ($q_{overland}$) or reaches the slow reservoir as preferential flow (q_{pref}). The process is governed by the parameter ρ_p. Recharge into groundwater can occur on rainy days.

$$q_{overland} = (P_{eff,tot} - q_{soil}) \cdot \rho_p \tag{15}$$

$$q_{pref} = (P_{eff,tot} - q_{soil}) \cdot (1 - \rho_p) \tag{16}$$

$$S_{soil} = S_{soil} + q_{soil} \tag{17}$$

The transpiration of the unsaturated zone is only limited by the potential evaporation if the water stored in soil is greater than the proportion F_{evap} of $S_{soil,max}$. Below, the flux is reduced linearly until reaching 0 for $S_{soil} = 0$. The underlying reason is that the more water is stored in the soil the more water is stored in large pores, which plants can easier access. The less water stored, the more water is stored in small pores which cannot be fully used by the plants for transpiration.

$$E_{soil} = (E_{pot} - E_{int}) \cdot min(\frac{S_{soil}}{S_{soil,max} \cdot F_{evap}}, 1) \tag{18}$$

In the riparian HRU, water can also enter the soil from the slow reservoir via a flux q_{rip} (Eq. 20). The excess water flows into the fast reservoir (Eq. 21).

$$\frac{dS_{soil,rip}}{dt} = q_{soil,rip} - E_{soil} \tag{19}$$

$$q_{soil,rip} = min((1 - C_r) \cdot (P_{eff,tot} + q_{rip}), S_{soil,max} - S_{soil}) \tag{20}$$

$$q_{over} = P_{eff,tot} + q_{rip} - q_{soil,rip} \tag{21}$$

A.4 Fast Reservoir

The change in storage of the fast reservoir increases with water that does not enter the soil but runs off on the surface and decreases by discharge into the river (Eq. 22). It is expressed as a linear response reservoir with a reservoir constant (k_{fast}), so that each time step a fixed percentage of water discharges into the river (Eq. 23).

$$\frac{dS_{fast}}{dt} = q_{overland} - q_{fast} \tag{22}$$

$$q_{fast} = k_{fast} \cdot S_{fast} \tag{23}$$

A.5 Slow Reservoir

The change in slow reservoir is defined by the incoming preferential flow of all hill-slope HRUs and the outflow q_{slow} (Eq. 24), which depends on the reservoir constant k_{slow} (Eq 25). Losses to deep ground water are neglected because it is assumed that the amount is so small that increasing the complexity of the model is not justified.

$$\frac{dS_{slow}}{dt} = q_{pref,bare} + q_{pref,forest} + q_{pref,grass} - q_{slow} \tag{24}$$

$$q_{slow} = k_{slow} \cdot S_{slow} \tag{25}$$

Part of the outflow q_{slow} enters the unsaturated zone of the riparian HRU, governed by the parameter ρ_{rip} (Eq. 26). The remaining water contributes to the river discharge (Eq. 27).

$$q_{rip} = \rho_{rip} \cdot q_{slow} \tag{26}$$

$$q_{base} = (1 - \rho_{rip}) \cdot q_{slow} \tag{27}$$

A.6 River Discharge

The river discharge at each time step is defined by the weighted sum of the outflows of the fast reservoirs of each HRU (q_{fast}) and the outflow of the slow reservoir (q_{base}).

$$Q_{river} = \sum_{i=1}^{HRU} q_{fast,i} + q_{base} \cdot (A_{bare} + A_{forest} + A_{grass}) \tag{28}$$

A lag function to account for channel routing was not implemented in the model. The longest catchment (Gailtal) is 60km long. Assuming a flow velocity of 1 m/s, it would take maximum 17h for the water to get routed to the outlet of the catchment. As time steps of one day are used, channel routing can be neglected.

Loss Term Pitztal In the Pitztal water is diverted to a reservoir in the Kaunertal close by. The exact amount of water diversion at each time step is unknown but the maximum amount diverted is 12.1 m^3/s. It is assumed that during low discharges almost no water is diverted, whereas at high discharges the maximum amount is diverted. Thus, an exponential relationship with an upper boundary was assumed (Eq. 29). This results in an additional parameter that has to be calibrated ($loss$) which can range from 0.01 to 0.08.

$$Q_{loss} = \begin{cases} loss \cdot Q_{river}^2 & \text{if } loss \cdot Q_{river}^2 \leq 12.1 \\ 12.1 & \text{if } loss \cdot Q_{river}^2 > 12.1 \end{cases} \tag{29}$$

$$Q_{river,real} = Q_{river} - Qloss \tag{30}$$

B Parameters

In order to reduce the number of parameters, most parameters were kept constant across HRUs. Only parameters for landscape dependent processes, i.e. interception and soil storage, were defined individually per HRU (see Table B). Prior parameter ranges were determined based on literature (Prenner et al., 2018; Gao et al., 2014; Girons Lopez et al., 2020) and further improved based on first calibration runs in order to decrease the possible parameter space and improve calibration. To ensure parameter combinations of HRUs are in line with the perception of the system, they were constrained based on Gharari et al. (2014). The interception capacity of forest has to be larger than of grassland or of the riparian zone due to a higher Leaf Area Index of forests (Eq. 31 & 32). The soil storage capacity is constrained based on the assumption that larger plants have larger roots and a higher water demand and thus need more soil and a larger soil storage. Moreover, a larger soil storage capacity of grassland than riparian zone is assumed due to high ground water levels near the river shore (Eq. 33 & 34). Lastly, the reservoir constants were constrained by the rate at which they discharge into the river (Eq. 35).

$$I_{max,forest} > I_{max,grass} \tag{31}$$

$$I_{max,forest} > I_{max,rip} \tag{32}$$

$$S_{soil,max,forest} > S_{soil,max,grass} > S_{soil,max,rip} \tag{33}$$

$$S_{soil,max,forest} > S_{soil,max,grass} > S_{soil,max,bare} \tag{34}$$

$$k_{fast,rip} > k_{fast} > k_{slow} \tag{35}$$

Table 1: Global prior parameter range for all catchments. For Pitztal the range for T_{thresh} was larger -2.5 to 2.5

	Global Parameters	**Unit**	**Min**	**Max**
T_{thresh}	Threshold Temperature	°C	-2	2
F_{melt}	Melt factor	mm/°C	1	6
M_M	Smoothness parameter for melt	°C	0.001	1.0
ρ_p	Share preferential flow	-	0.1	0.9
k_{fast}	fast hillslope constant	1/d	0.1	1.0
k_{slow}	slow constant	1/d	0.001	0.1
F_{evap}	Evapotranspiration control factor	-	0.4	0.8
	Bare Rock/ Sparse Vegetated			
$S_{soil,max,_{bare}}$	max. soil storage capacity	mm	1	50
β_{bare}	factor accounting for nonlinearity	-	0.1	2
	Forested Hillslope			
$I_{max_{forest}}$	max. Interception capacity	mm	1	3
$S_{soil,max,_{forest}}$	max. soil storage capacity	mm	50	500
β_{forest}	factor accounting for nonlinearity	-	0.1	2
	Grassland Hillslope			
$I_{max_{grass}}$	max. Interception capacity	mm	1	2
$S_{soil,max,_{grass}}$	max. soil storage capacity	mm	5	250
β_{grass}	factor accounting for nonlinearity	-	0.1	2
	Riparian Zone			
$I_{max_{rip}}$	max. Interception capacity	mm	1	3
$S_{soil,max,_{rip}}$	max. soil storage capacity	mm	5	250
β_{rip}	factor accounting for nonlinearity	-	0.1	2
$k_{fast,rip}$	fast riparian constant	1/d	0.2	3
ρ_{rip}	Share riparian flow	-	0.05	0.5

B.1 Objective Functions

In order to calibrate the model, it is necessary to compare the model output to discharge measurements based on so called objective functions. Due to high amount of parameters of the model it is necessary to use several objective functions to make sure that the model represents well the catchment behaviour. The overall performance of the model was assessed using the mean Euclidean Distance (D_e) from the perfect model fit (Hrachowitz et al., 2014) as shown in Eq. 36 where Obj_n denotes the objective functions and N the total number of objective functions. A perfect fit between modelled and observed signatures would result in $Obj_n = 1$.

$$D_e = \sqrt{\frac{\sum_{n=1}^{N}(1 - Obj_n)^2}{N}} \tag{36}$$

Nash Sutcliffe Efficiency A widely used objective function in hydrology is the Nash Sutcliffe Efficiency (NSE) (Eq. 37). The NSE ranges between 1 and -∞. A perfect fit would result in a NSE of 1. A value of zero indicates that the mean observed stream flow is the best estimation of the model. The NSE tends to overemphasizes peak flows because the deviations between the model and observed stream flow are squared. Therefore, it is necessary to use another objective function which is focused on the low flows. A good objective function for this purpose is the Log Nash-Sutcliffe efficiency (Eq. 38) because it is more sensitive to low flows than to peak flows.

$$NSE = 1 - \frac{\sum_{i=1}^{n}(Q_{Mod,i} - Q_{Obs,i})^2}{\sum_{i=1}^{n}(Q_{Obs,i} - \overline{Q_{Obs}})^2} \tag{37}$$

$$NSE_{log} = 1 - \frac{\sum_{i=1}^{n}(\log(Q_{Mod,i}) - \log(Q_{Obs,i}))^2}{\sum_{i=1}^{n}(\log(Q_{Obs,i}) - \log(\overline{Q_{Obs}}))^2} \tag{38}$$

Volumetric Efficiency The volumetric efficiency describes the fraction of water delivered at the proper time (Criss & Winston, 2008).

$$VE = 1 - \frac{\sum_{i=1}^{n}|Q_{Mod,i} - Q_{Obs,i}|}{\sum_{i=1}^{n} Q_{Obs,i}} \tag{39}$$

Flow Duration Curve A Flow Duration Curve plots the magnitude of daily discharges against the exceedence probability on any day. The flow duration curve of the logarithmic flows is calculated. The NSE between the observed and modelled flow duration curve is taken as objective function. As the timing of the flow is not considered for FDC, but only the magnitude, this objective function focuses on the magnitude of flows, disregarding a proper representation of timing.

Autocorrelation The autocorrelation is a measure of the "memory" of the catchment. If the memory is high, the correlation values should be high and the hydrograph is smooth. If the memory is low, the correlation values are low and the hydrograph has sharp peaks. The autocorrelation with a lag of 1 day is calculated (see Eq. 40) and the results of observed and modelled streamflow are compared using the relative error. As a another signature, the auto correlation values with a lag of 1 to 90 days were calculated. The resulting autocorrelation functions of the observed and modelled streamflow are compared using the NSE.

$$AC = \frac{\sum_{i=1}^{n}(Q_i - \overline{Q})(Q_{i+1} - \overline{Q})}{\sum_{i=1}^{n}(Q_i - \overline{Q})^2} \tag{40}$$

Monthly Runoff Coefficient The runoff coefficient is the ratio of total discharge to total precipitation. If the monthly runoff coefficient are correctly represented by the model, it means that the model is able to reproduce the amount of runoff and evaporation correctly. The following function is used to calculate the monthly runoff with n the number of days in the corresponding month. The runoff coefficients of all months are compared using the NSE.

$$R = \frac{\sum_{i=1}^{n} Q}{\sum_{i=1}^{n} P} \tag{41}$$

Snow Cover Using satellite derived snow cover images for calibration significantly improves correct representation of glaciers, snow and rain (Finger et al., 2015). Thus, MODIS satellite data is used to determine the daily area fraction of the catchments covered by snow ($a_{obs,i}$) which is compared to the modeled area fraction covered by snow ($a_{mod,i}$), where an SC of one indicates a perfect fit.

$$SC = \frac{1}{n}\sum_{i=1}^{n}(1 - |a_{mod,i} - a_{obs,i}|) \tag{42}$$

C Calculation of Analysis of Change

C.1 Timing of Maximum/Minimum Flow

The mean timing of annual maximum and minimum flow over 30 years was calculated using the approach of circular statistics (e.g. Young et al. (2000); Blöschl et al. (2017). Therefore, the date of occurence (D_i) has to be converted to an angle (Eq. 43) where $Lenyr$ denotes the number of days in each year. The date of occurrence for the maximum annual runoff is defined as the date of maximum daily discharge in a calender year. The date of minimum annual flows is defined as the first day of the seven consecutive days with lowest flows in the time period from June to May.

$$\theta_i = D_i \cdot \frac{2\pi}{Lenyr_i} \tag{43}$$

The mean date of occurrence over the 30 year time period is calculated by

$$\overline{D} = \begin{cases} \tan^{-1}(\frac{\overline{y}}{\overline{x}}) \cdot \frac{\overline{Lenyr}}{2\pi} & \overline{x} > 0, \overline{y} \geq 0 \\ (\tan^{-1}(\frac{\overline{y}}{\overline{x}}) + \pi) \cdot \frac{\overline{Lenyr}}{2\pi} & \overline{x} \leq 0 \\ (\tan^{-1}(\frac{\overline{y}}{\overline{x}}) + 2\pi) \cdot \frac{\overline{Lenyr}}{2\pi} & \overline{x} > 0, \overline{y} < 0 \end{cases} \tag{44}$$

using

$$\overline{x} = \frac{1}{n}\sum_{i=1}^{n}\cos\theta_i \tag{45}$$

$$\overline{y} = \frac{1}{n}\sum_{i=1}^{n}\sin\theta_i \tag{46}$$

$$\overline{Lengyr} = \frac{1}{n}\sum_{i=1}^{n}Lengyr_i \tag{47}$$

For calculating the distribution of the date of occurrences over the time period of 30 years, the year was divided into bins of 15 days, so 25 bins in total, with the last bin containing DOY > 360, so only 5 or 6 days. The fraction of occurrence per time bin was calculated as follows:

$$p_{15days} = \frac{\sum_{i=1}^{30} D_i}{30} \tag{48}$$

C.2 Magnitude of Maximum Annual Flow

In addition to calculating the mean magnitude of annual maximum flow, the distribution of magnitudes of annual maximum flow over 30 years was determined. Therefore, the magnitudes were ranked, from the highest (i=1) to lowest (i=30) annual maximum flow magnitude. The exceedance probability (p) was calculated, where N denotes the total number of observations, which is in this case 30.

$$p = \frac{i}{N+1} \tag{49}$$

The return period (T_a) was calculated using the exceedance probability

$$T_a = \frac{1}{p} \tag{50}$$

The magnitudes in relation to the return periods were analysed by calculating the absolute and relative change of magnitude for each return period.

C.3 Magnitude Minimum Flows

Next to the lowest runoff in the year calculated as moving average of 7 consecutive days, the Q_{90} of the flow duration curve was used as threshold value to determine low flows. The monthly deficit (D_f) was calculated as follows:

$$D_f = \frac{\sum_{i=1}^{N}(Q_{90} - Q_i)}{30} \tag{51}$$

where N denotes the total number of days within the time period, where $Q < Q_{90}$ in the specific month. The total number of days below the Q_{90} threshold per month was computed by $\frac{N}{30}$.

D Calibration & Evaluation

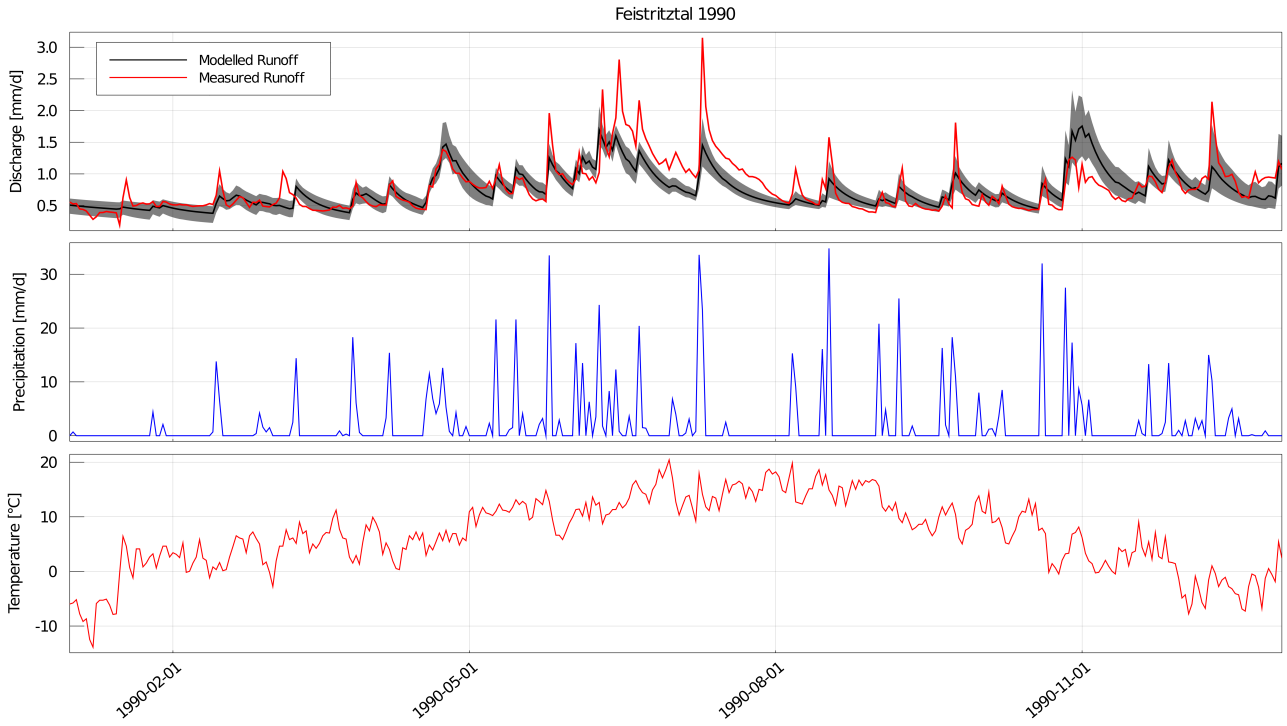

Figure D.1: Feistritztal 1990: Comparison of measured and modelled runoff, also showing the corresponding precipitation and temperature, black line indicates mean modelled runoff using best parameter sets, shaded area shows the uncertainty of best parameter sets.

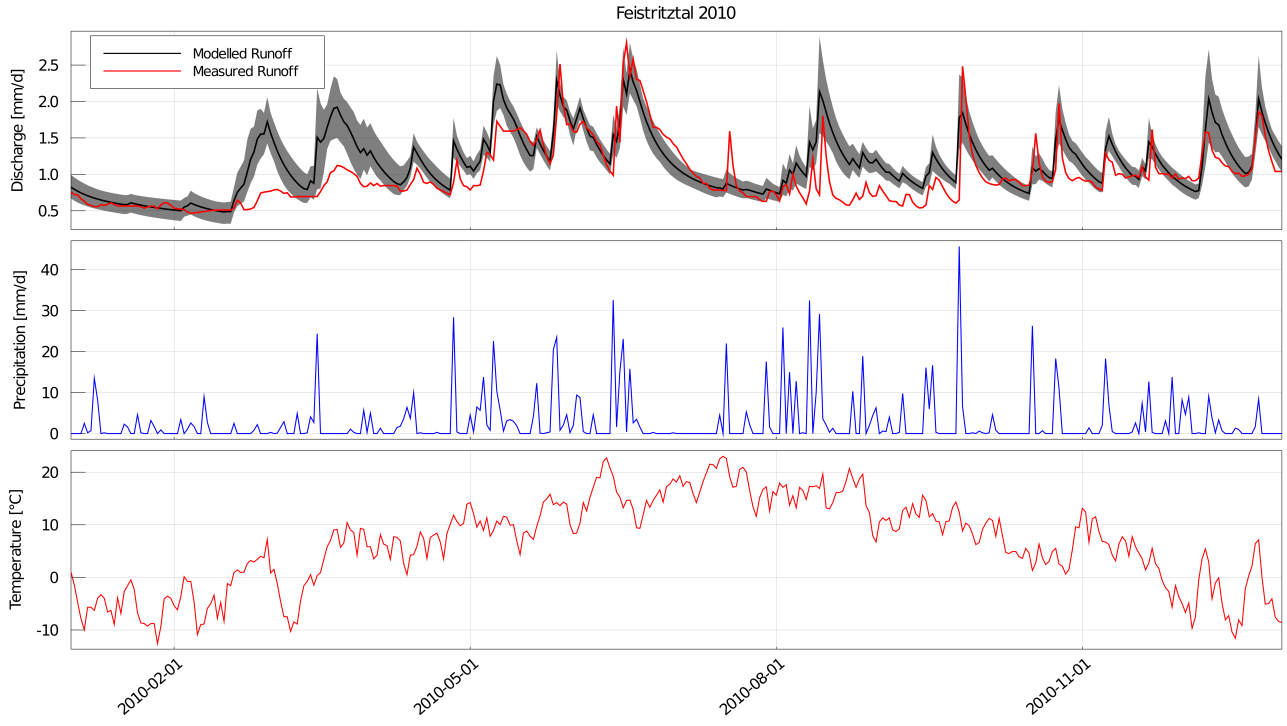

Figure D.2: Feistritztal 2010: Comparison of measured and modelled runoff, also showing the corresponding precipitation and temperature, black line indicates mean modelled runoff using best parameter sets, shaded area shows the uncertainty of best parameter sets.

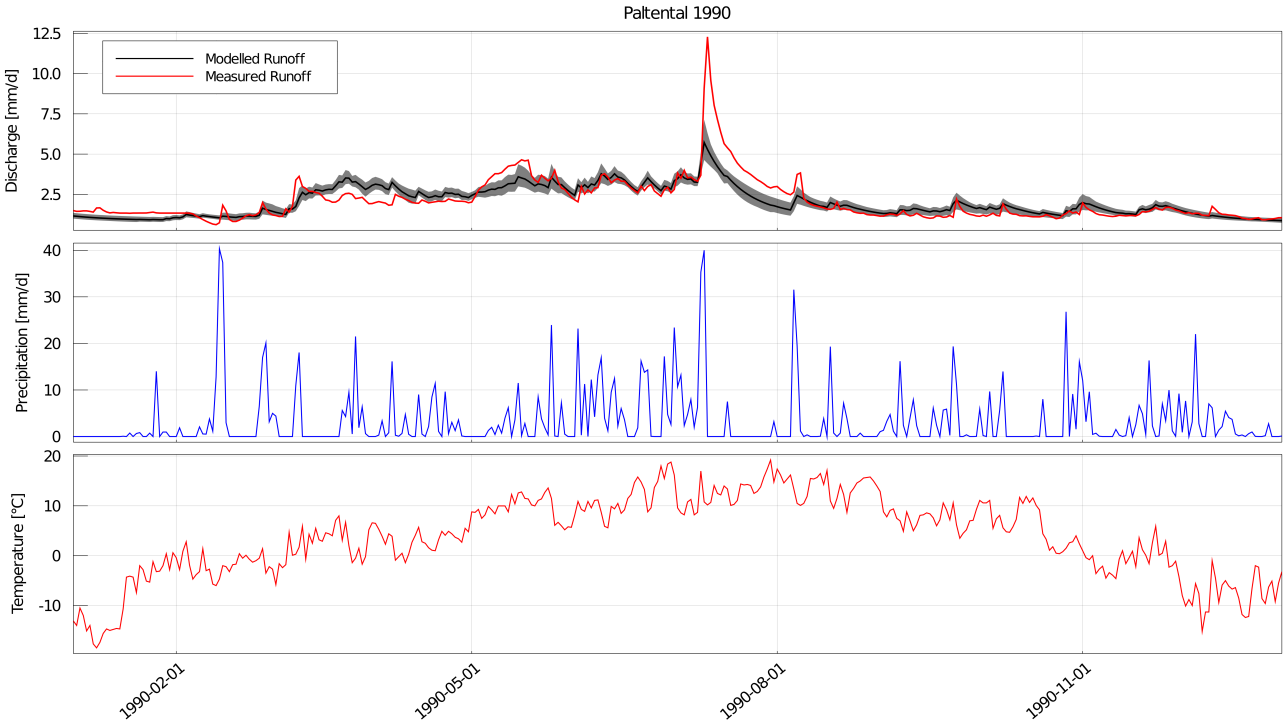

Figure D.3: Paltental 1990: Comparison of measured and modelled runoff, also showing the corresponding precipitation and temperature, black line indicates mean modelled runoff using best parameter sets, shaded area shows the uncertainty of best parameter sets.

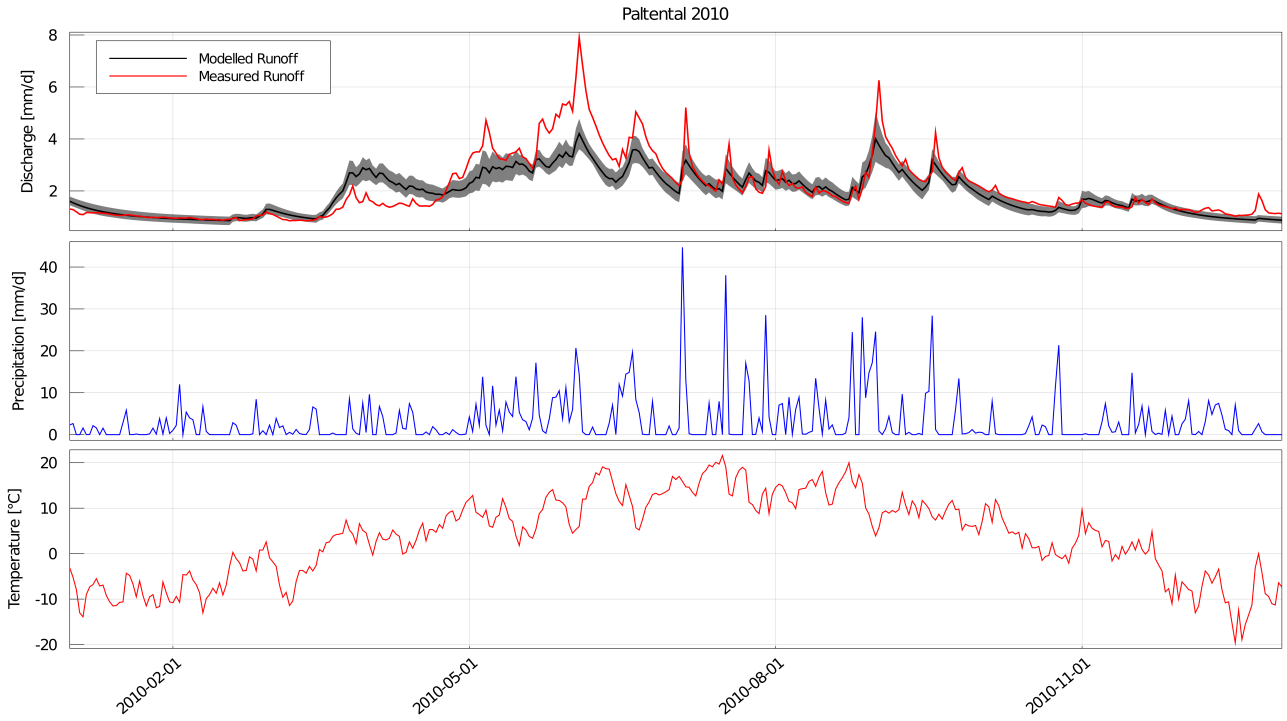

Figure D.4: Paltental 2010: Comparison of measured and modelled runoff, also showing the corresponding precipitation and temperature, black line indicates mean modelled runoff using best parameter sets, shaded area shows the uncertainty of best parameter sets.

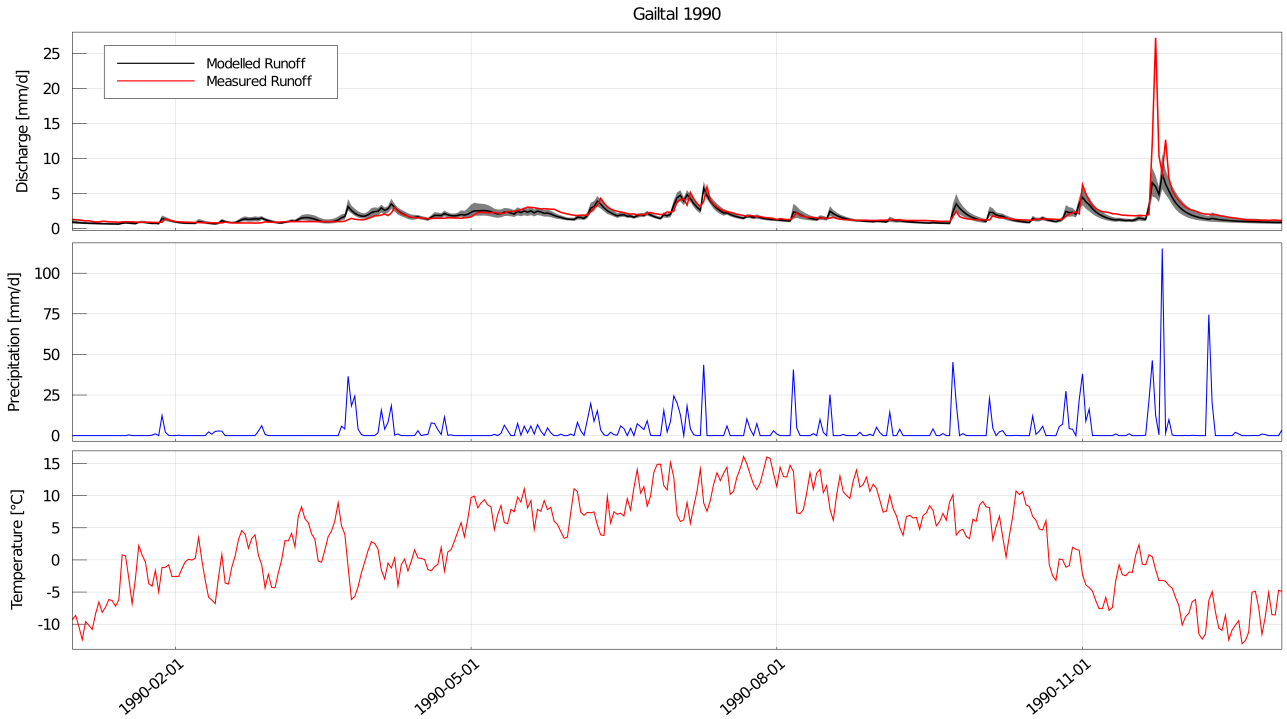

Figure D.5: Gailtal 1990: Comparison of measured and modelled runoff, also showing the corresponding precipitation and temperature, black line indicates mean modelled runoff using best parameter sets, shaded area shows the uncertainty of best parameter sets.

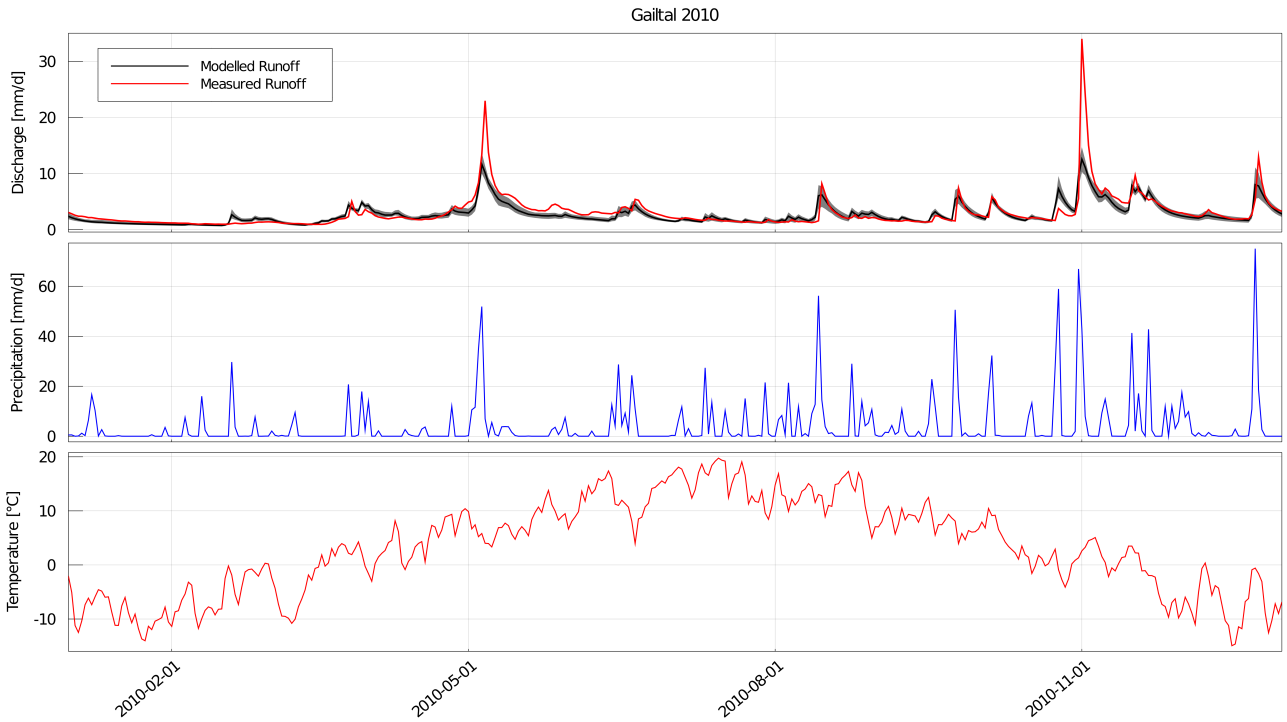

Figure D.6: Gailtal 2010: Comparison of measured and modelled runoff, also showing the corresponding precipitation and temperature, black line indicates mean modelled runoff using best parameter sets, shaded area shows the uncertainty of best parameter sets.

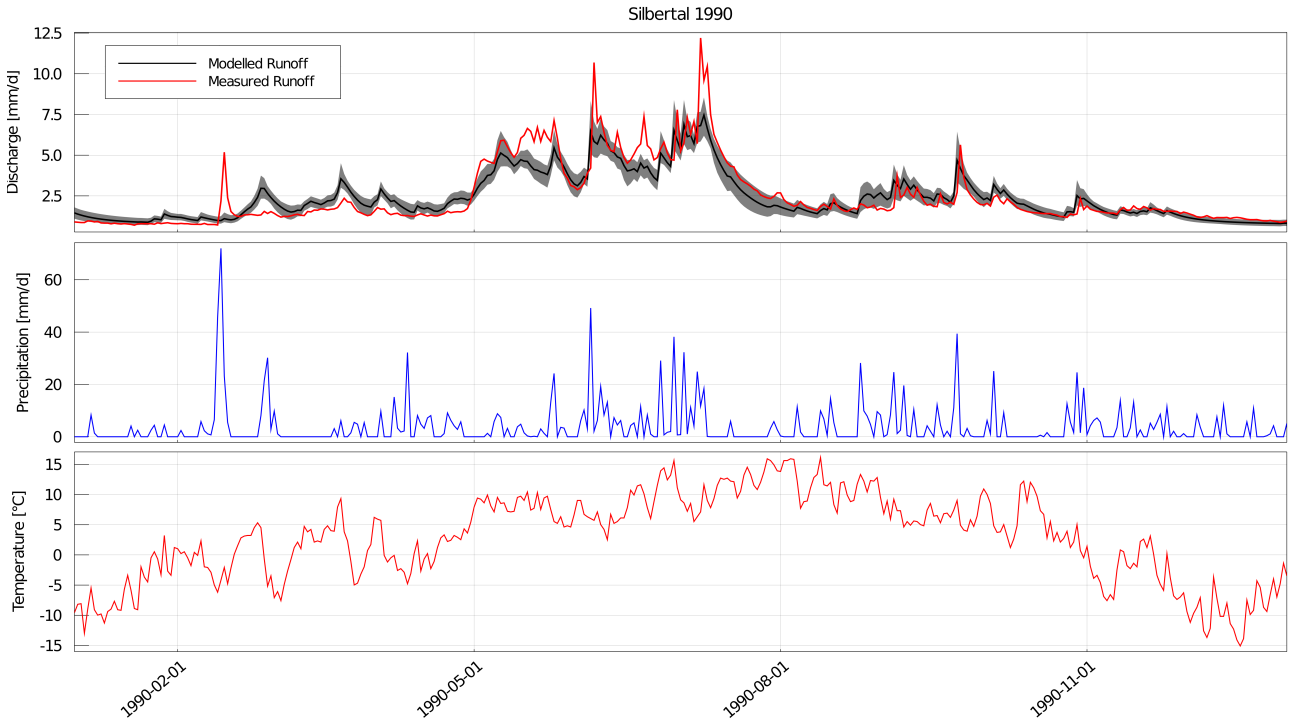

Figure D.7: Silbertal 1990: Comparison of measured and modelled runoff, also showing the corresponding precipitation and temperature, black line indicates mean modelled runoff using best parameter sets, shaded area shows the uncertainty of best parameter sets, the measured runoff was scaled to match Budyko framework.

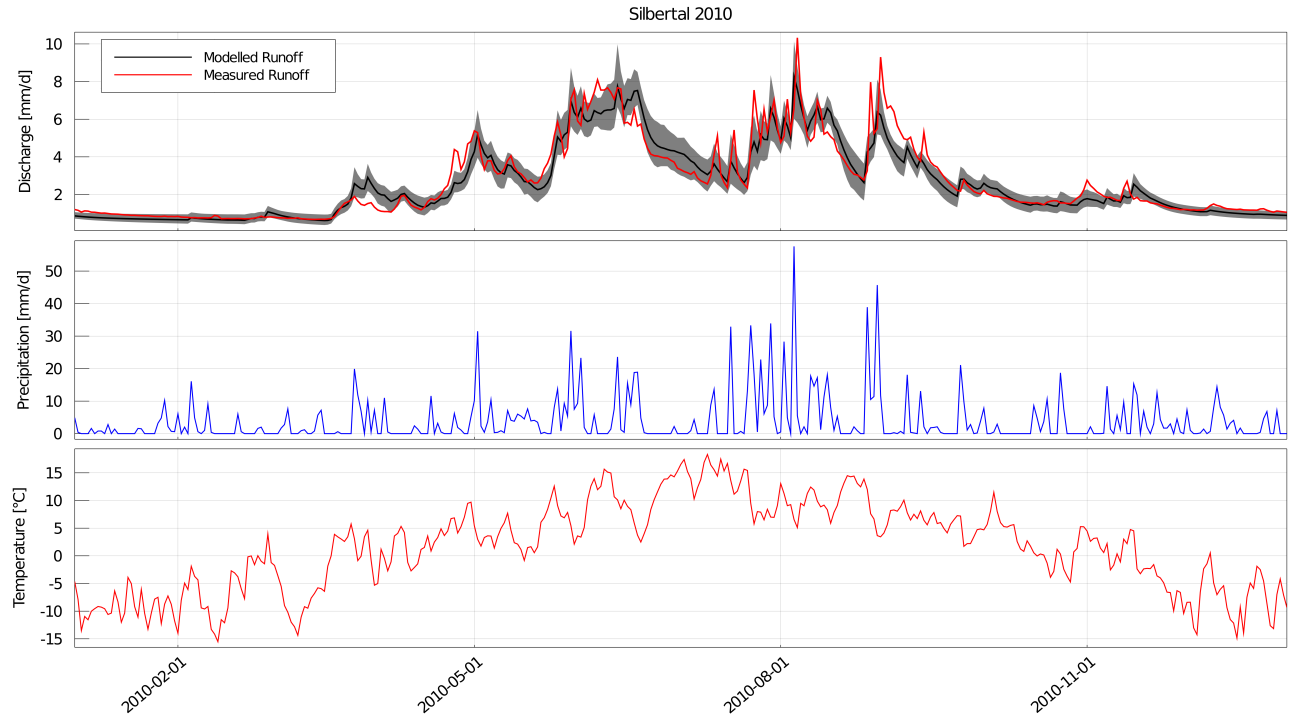

Figure D.8: Silbertal 2010: Comparison of measured and modelled runoff, also showing the corresponding precipitation and temperature, black line indicates mean modelled runoff using best parameter sets, shaded area shows the uncertainty of best parameter sets, the measured runoff was scaled to match Budyko framework.

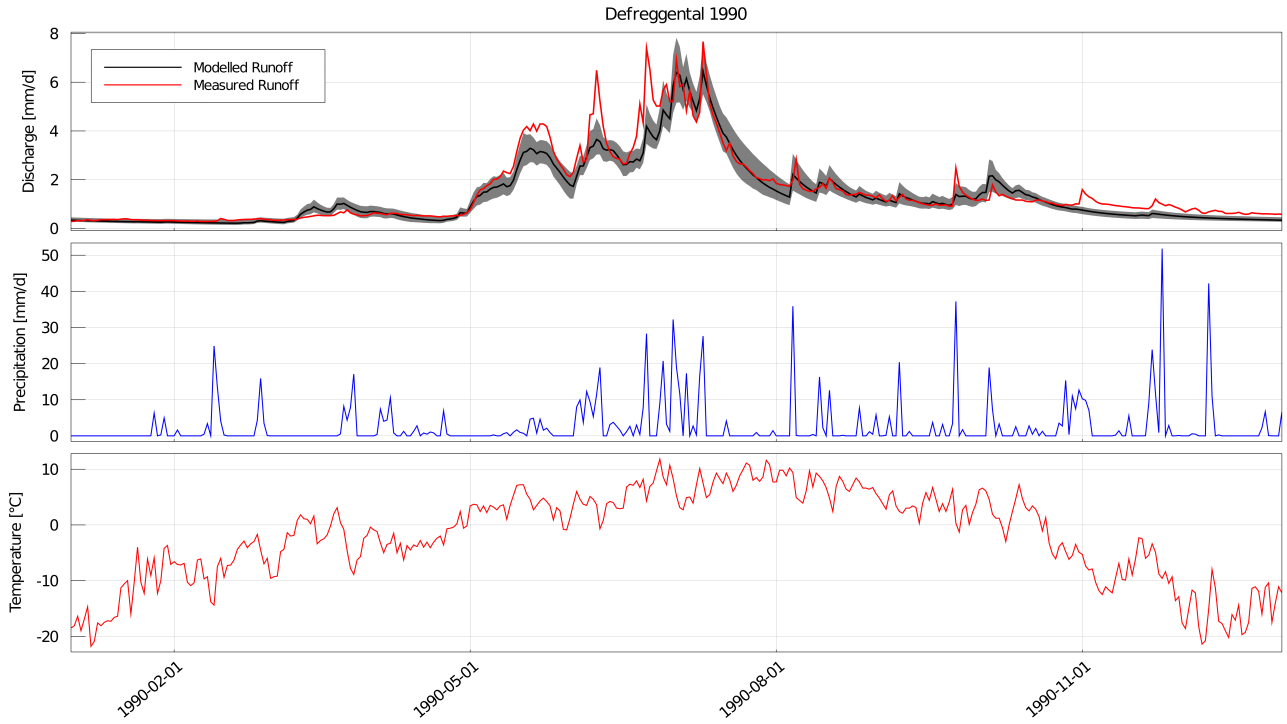

Figure D.9: Defreggental 1990: Comparison of measured and modelled runoff, also showing the corresponding precipitation and temperature, black line indicates mean modelled runoff using best parameter sets, shaded area shows the uncertainty of best parameter sets, the measured runoff was scaled to match Budyko framework.

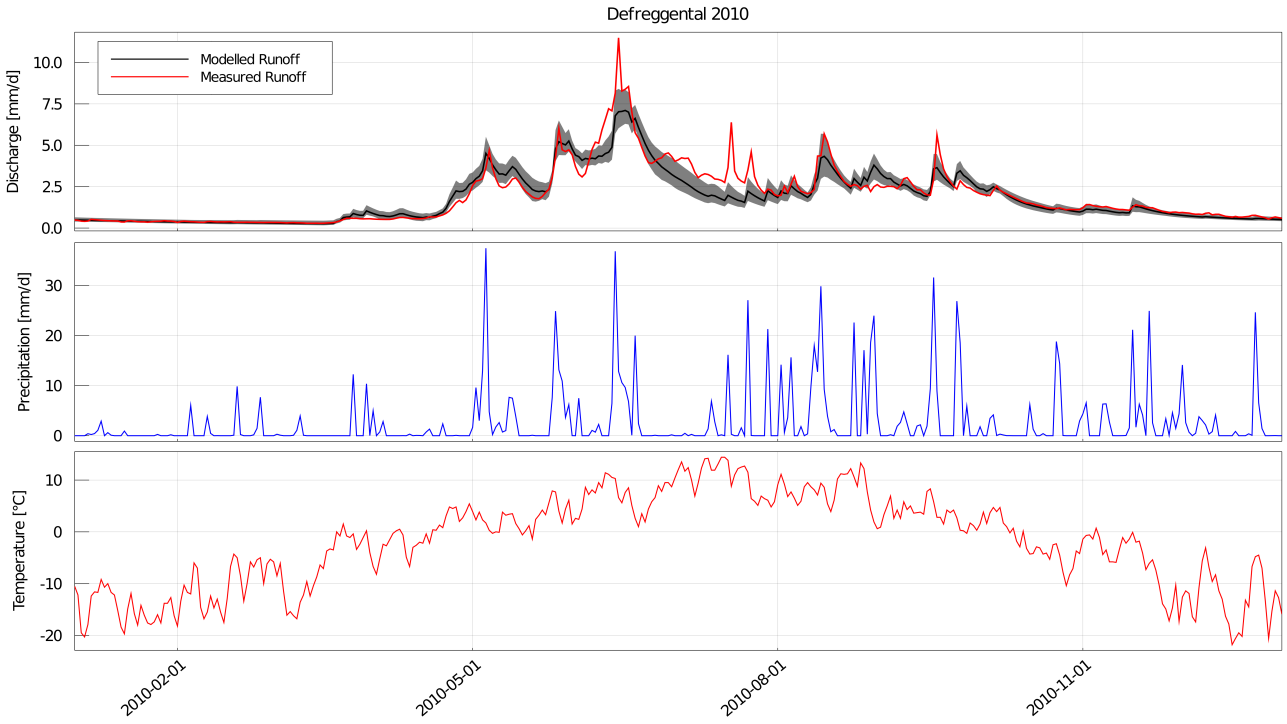

Figure D.10: Defreggental 2010: Comparison of measured and modelled runoff, also showing the corresponding precipitation and temperature, black line indicates mean modelled runoff using best parameter sets, shaded area shows the uncertainty of best parameter sets, the measured runoff was scaled to match Budyko framework.

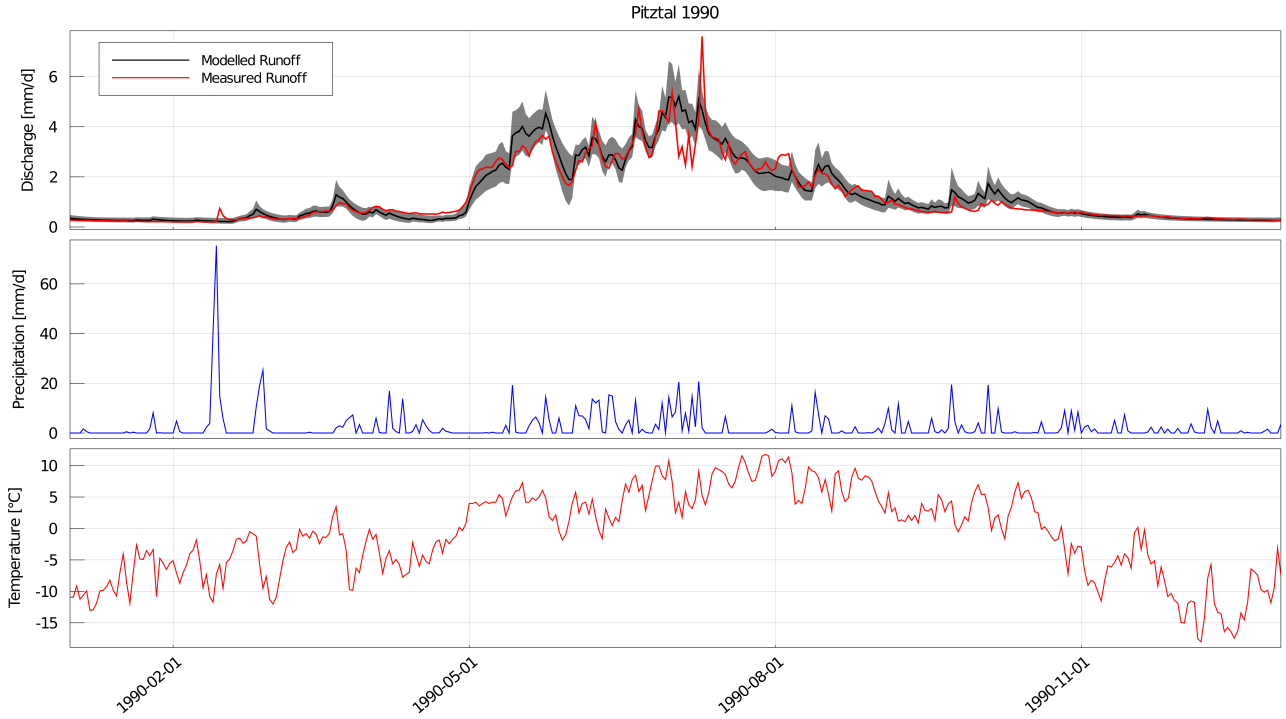

Figure D.11: Pitztal 1990: Comparison of measured and modelled runoff, also showing the corresponding precipitation and temperature, black line indicates mean modelled runoff using best parameter sets, shaded area shows the uncertainty of best parameter sets.

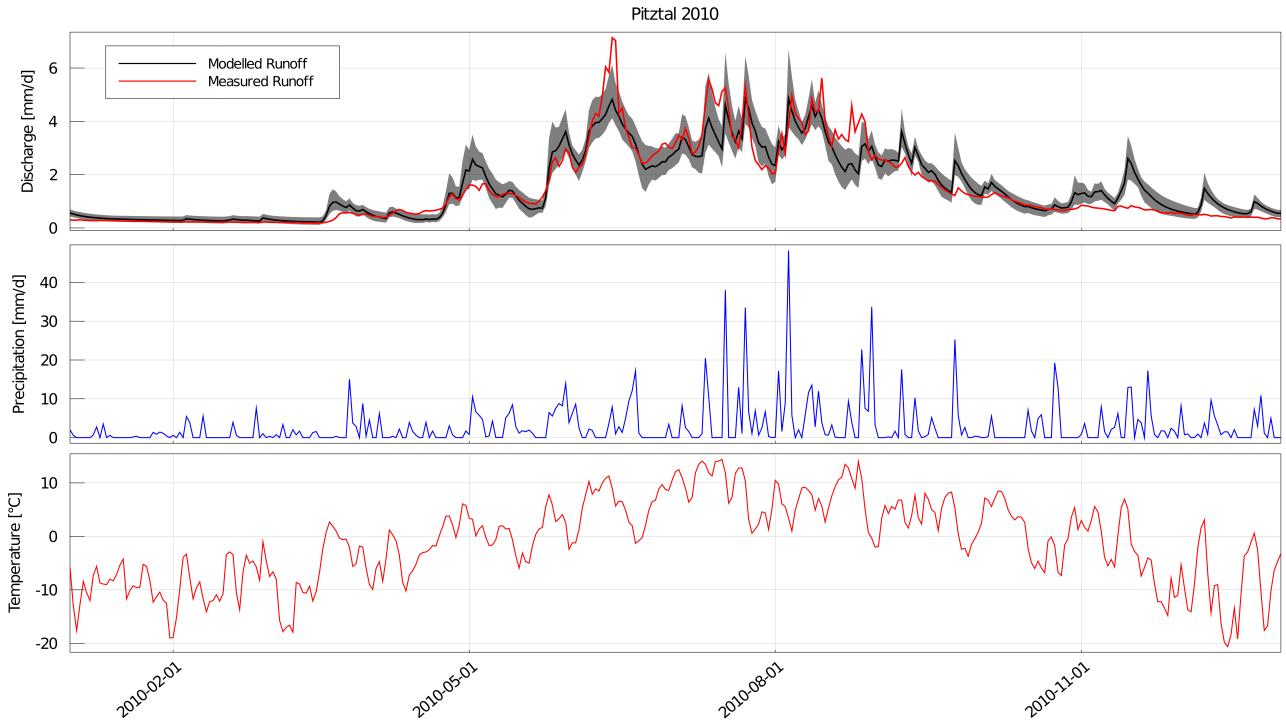

Figure D.12: Pitztal 2010: Comparison of measured and modelled runoff, also showing the corresponding precipitation and temperature, black line indicates mean modelled runoff using best parameter sets, shaded area shows the uncertainty of best parameter sets.

E Measured Data vs. Climate Simulations in the Past

The following plots show the comparison of measured data and climate projections for every catchments (Figure E-E). Yearly extreme events, i.e. maximum precipitation, maximum/minimum discharge, are compared using empirical cumulative distribution functions (ECDF) to show the distribution of magnitudes and timing over a 22 to 30 year time period in the past, depending on the catchment. On the right, monthly temperature and precipitation of measured data (left) and climate projections (right) are compared using boxplots. The lower right plot displays a comparison of mean monthly runoff over the time period using measured data as forcing for the hydrological model (left) or using climate projections as forcing (right). The observed mean monthly runoff is also shown as a black X.

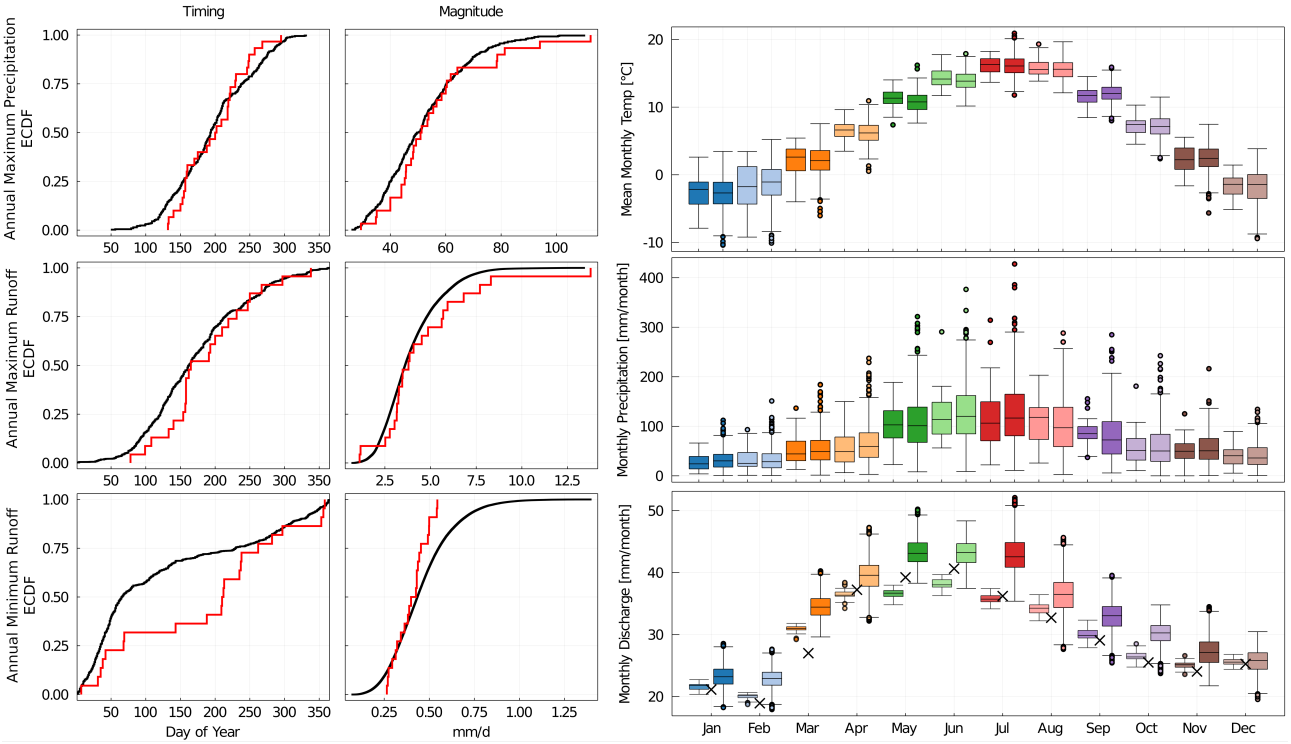

Figure E.13: Comparison of measured data and climate projections in the Feistritztal. Comparison of annual extremes on the left, red: observed data, black: climate projections. On the right, the comparison of monthly data is shown.

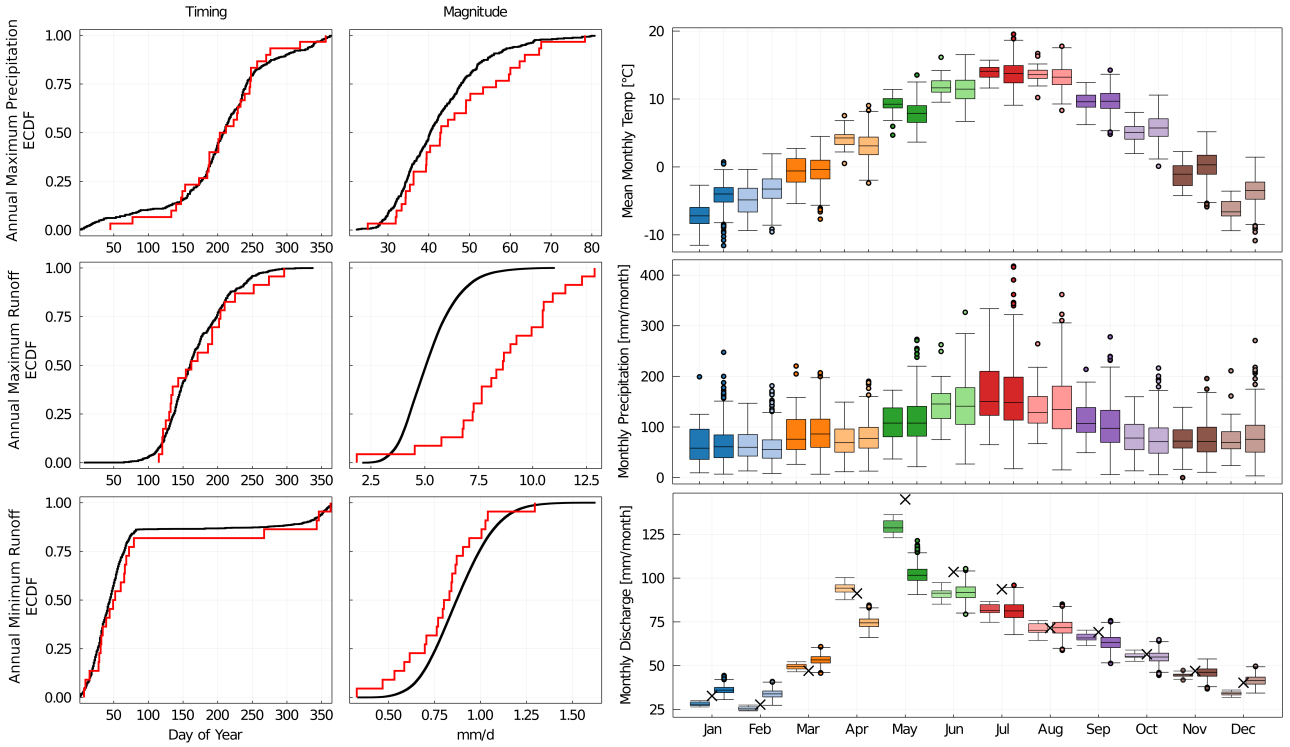

Figure E.14: Comparison of measured data and climate projections in the Paltental. Comparison of annual extremes on the left, red: observed data, black: climate projections. On the right, the comparison of monthly data is shown.

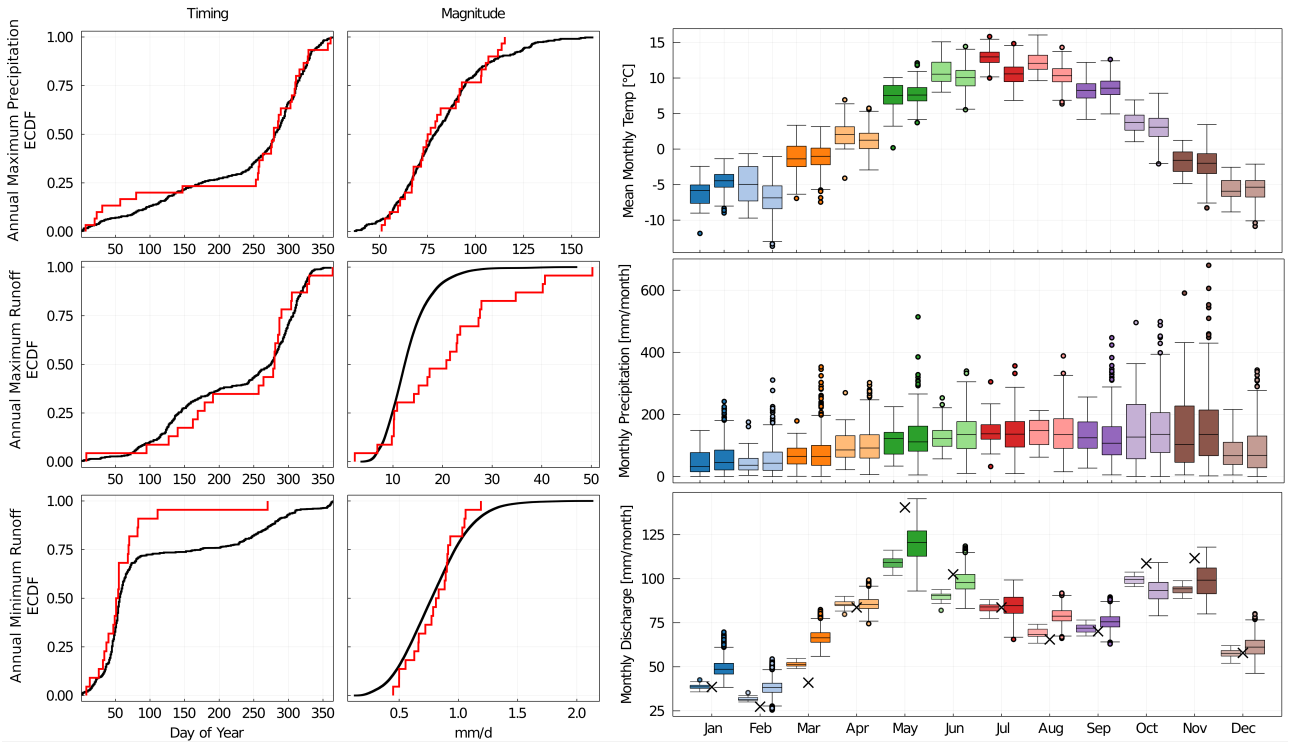

Figure E.15: Comparison of measured data and climate projections in the Gailtal. Comparison of annual extremes on the left, red: observed data, black: climate projections. On the right, the comparison of monthly data is shown.

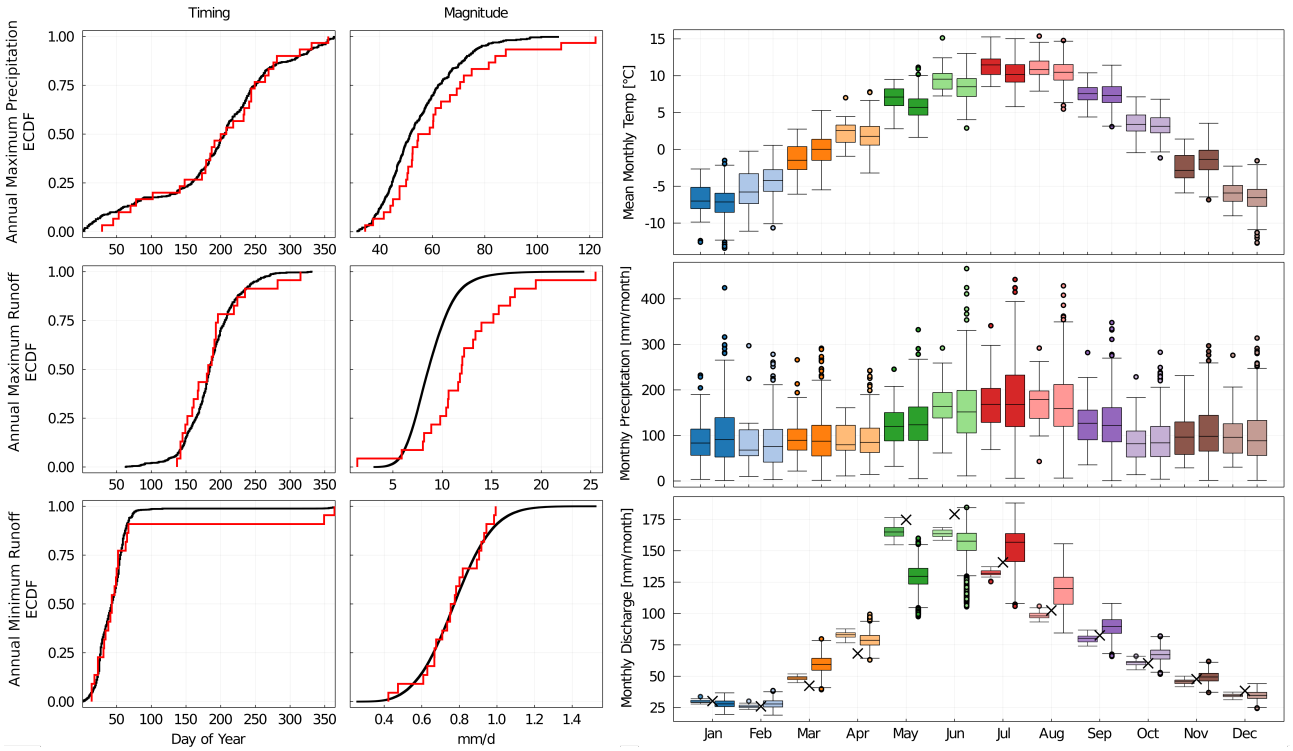

Figure E.16: Comparison of measured data and climate projections in the Silbertal. Comparison of annual extremes on the left, red: observed data, black: climate projections. On the right, the comparison of monthly data is shown.

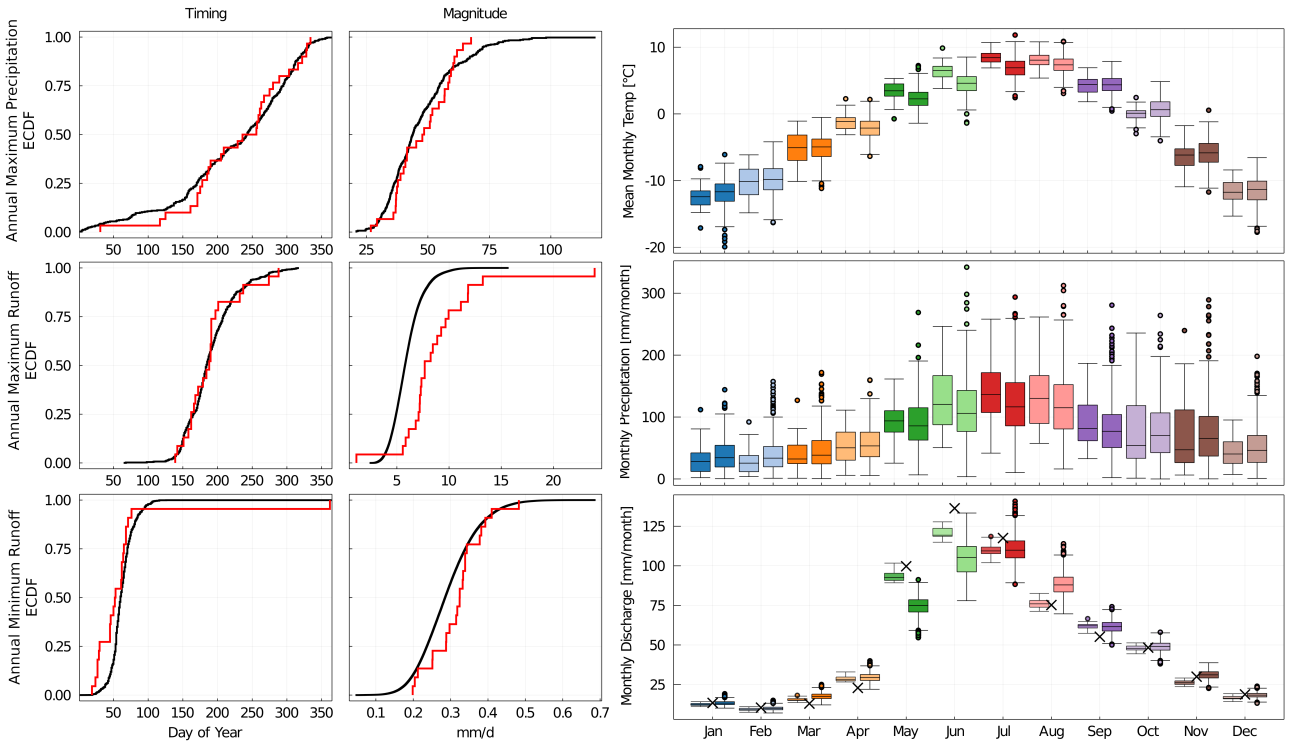

Figure E.17: Comparison of measured data and climate projections in the Defreggental. Comparison of annual extremes on the left, red: observed data, black: climate projections. On the right, the comparison of monthly data is shown.

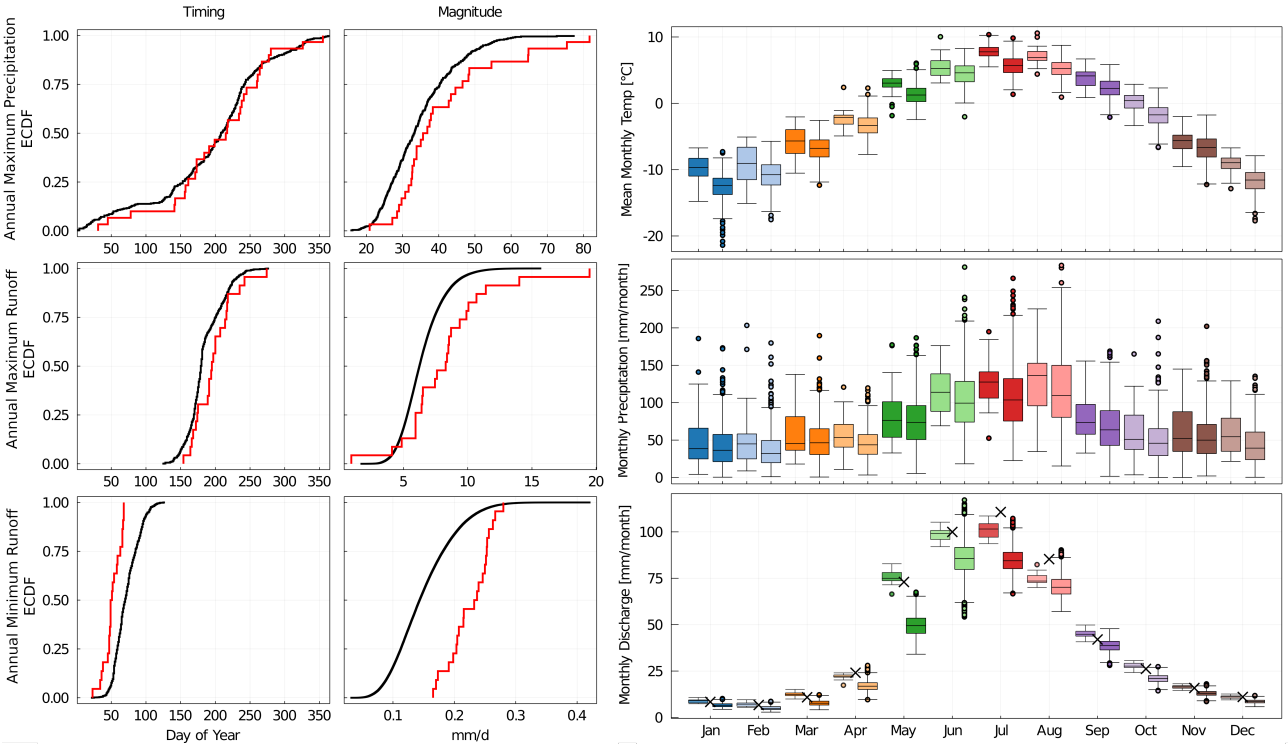

Figure E.18: Comparison of measured data and climate projections in the Pitztal. Comparison of annual extremes on the left, red: observed data, black: climate projections. On the right, the comparison of monthly data is shown.

F Results Additional Plots

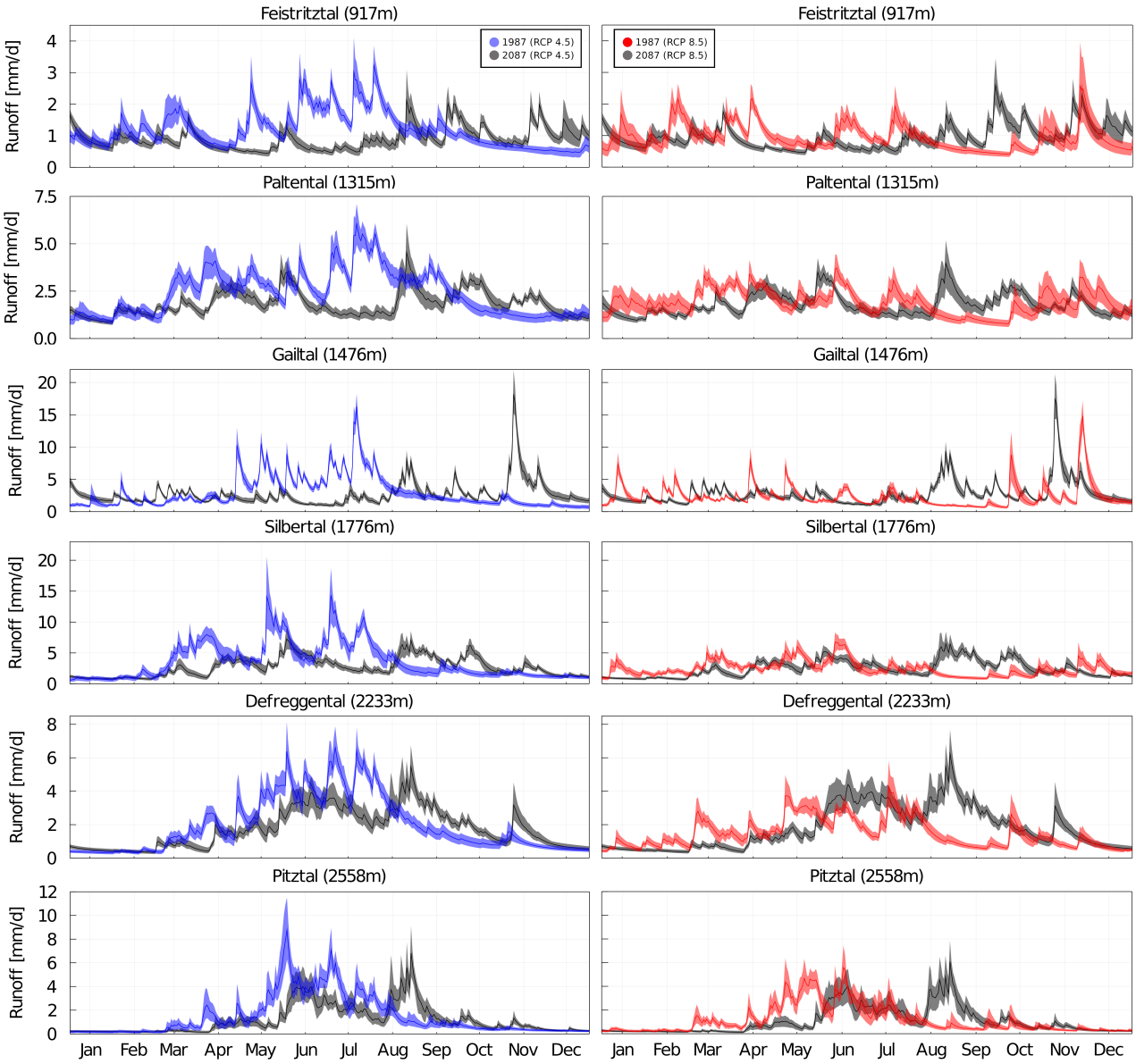

Figure F.19: Runoff in past and future of all catchments illustrated by hydrographs of 1987 and 2087 under RCP 4.5 and RCP 8.5 for Projection-14. The shaded area is the range of runoffs modelled by the best parameter sets, the line the mean. For Pitztal simulations without the loss term are used.

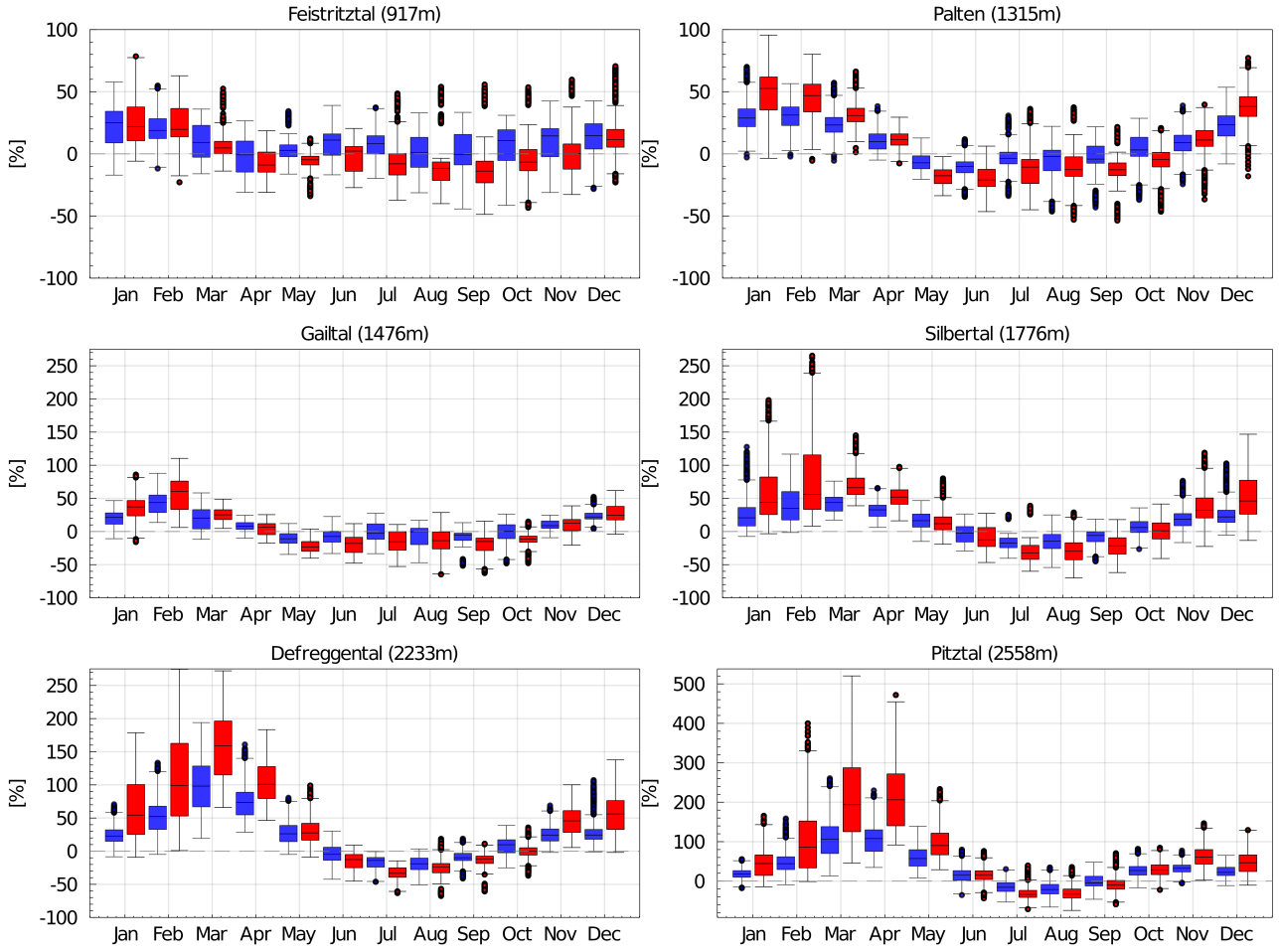

Figure F.20: Relative changes in mean monthly discharge of all catchments, blue indicates RCP 4.5, red RCP 8.5, mean elevation in brackets. Note the different scales.

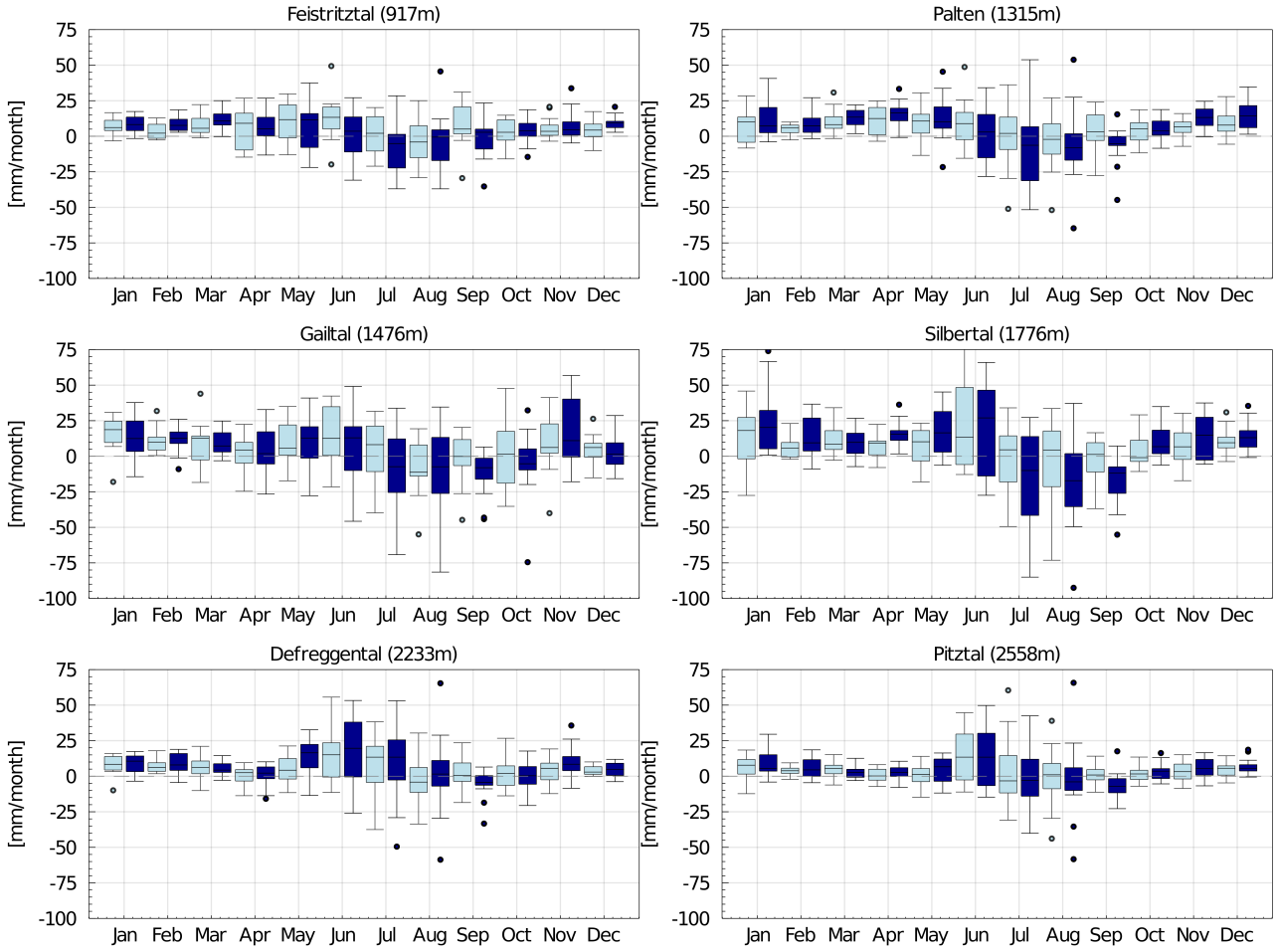

Figure F.21: Absolute changes in mean monthly precipitation of all catchments, light blue indicates RCP 4.5, dark blue RCP 8.5, mean elevation in brackets. Note the different scales.